A Study of Chameleon-Photon Mixing From Pulsars

Author

Mr. Muzikayise E. Sikhonde

Student number: Skhmuz002

Supervisor

Dr. Amanda Weltman

Senior Lecturer

Department of Mathematics and Applied Mathematics

University of Cape Town.

Thesis presented for the degree of Master of Science in the

Department of Mathematics and Applied Mathematics

Faculty of Science

University of Cape Town

July 23, 2012

A Study of Chameleon-Photon Mixing From Pulsars

Author

Mr. Muzikayise E. Sikhonde

Student number: Skhmuz002

Supervisor

Dr. Amanda Weltman

Senior Lecturer

Department of Mathematics and Applied Mathematics

University of Cape Town

A thesis submitted in partial fulfilment of the requirement for the degree of

M.Sc. Astrophysics and Space Science

External Examiner Signature:.....

Thesis Supervisor Signature:.....

Department of Mathematics and Applied Mathematics

Faculty of Science

University of Cape Town

Abstract

A number of solutions to the dark energy problem have been proposed in literature, the simplest is the cosmological constant Λ. The cosmological constant lacks theoretical explanation for its extremely small value, thus dark energy is more generally modelled as a quintessence scalar field rolling down a flat potential. For the quintessence scalar field to be evolving on cosmological scales its mass must be of order H_0 , which is the present value of the Hubble constant. A scalar field ϕ whose mass varies with the background energy density was proposed by Khoury and Weltman in 2003. This scalar field can evolve cosmologically while having coupling to different matter fields of order unity. Such a scalar field also couples to photons in the presence of an external magnetic field via the ϕF^2 interaction, where F stands for the electromagnetic field strength tensor. The chameleon-photon coupling of this nature causes a conversion of photons to light Chameleon particles and vice versa. In this work we investigate this effect on pulsars, and we constrain the chameleon-photon coupling constant in this theory.

Acknowledgements

I would like to thank my supervisor Dr. Amanda Weltman for proposing this project and for her encouragement and support through discussions during the course of the project. And I am thankful to Dr. De-Chang Dai for his input at the beginning of the project by helping me with some conceptual issues. I would also like to thank my family and friends for supporting and believing in me through the course of this project. I am grateful to the south African NRF-SKA scholarship programme for their financial support for the past two years to make this project possible. I acknowledge the National Astrophysics and Space Science programme (NASSP) and the University of Cape Town (UCT) for providing their research facilities in support of this project.

Dedications

I dedicate this work to my mother

Contents

List of Figures

1 Introduction

1.1 Dark Energy

1.1.1 The Cosmological Constant

In 1917, Albert Einstein introduced the cosmological constant Λ in order to obtain a static universe from his field equation [6], he was motivated by its effects on Newtonian theory which solved the problem of infinities in cosmology. It follows directly from the Raychaudhuri equation that a static universe requires a positive cosmological constant as long as the energy requirement that $\rho + 3p > 0$ is satisfied, with ρ and p being the energy density and pressure respectively. In 1930 Eddington showed that the Λ dominated Einstein universe was unstable, this follows from the Raychaudhuri equation for a static universe with the condition that $\rho + p > 0$ [7].

By 1960 Thackeray and Baade had revised the distance estimates that lead to the revised Hubble constant to resolve the problem of the age of the universe and there was no need for the cosmological constant. In 1967 Zeldovich investigated the stress-energy tensor of the dynamic vacuum from quantum field theory [8, 9], which behaves like an effective cosmological constant, and can arise as an asymptotic form of the energy density of a scalar field. In 1980 this idea became the basis of the inflationary paradigm proposed by Guth [10].

Classically the effective energy density of a scalar field will take the form of a perfect fluid with energy density $\rho = \frac{1}{2}\dot{\phi}^2 + V(\phi)$ and pressure $p = \frac{1}{2}\dot{\phi}^2 - V(\phi)$ which obeys the

Klein-Gordon equation $\ddot{\phi} + 3H\dot{\phi} + \frac{\partial V}{\partial \phi} = 0$ where ϕ, $V(\phi)$ and H are the scalar field, its potential and the Hubble parameter respectively, such that its energy and momentum are conserved. In the slow-roll approximation ($\dot{\phi}^2 \ll V(\phi) \Rightarrow \rho + p \sim 0, \rho + 3p = 2[\dot{\phi}^2 - V(\phi)]$) this field behaves like a cosmological constant, and can cause an exponential expansion at early times if the slow-roll condition lasts long enough [10].

In the late nineties, the cosmological constant was revived through the discovery that the dynamics of the late time expansion of the universe was dominated by the cosmological constant, through the Hubble diagram for supernovae in distant galaxies, it was determined that the universe is expanding and accelerating. This could be explained by a positive cosmological constant Λ, or the energy density of a scalar field that is quintessence [11, 12]. From astrophysical modeling the current best fit models to all the observations have values of approximately $\Omega_m \sim 0.3$, $\Omega_\Lambda \sim 0.7$ and $\Omega_k \sim 0$, for the effective densities of all matter, the cosmological constant and the curvature respectively.

The physics behind the cosmological constant is not presently understood, hence illuminating the nature of the underlying physics of the cosmological constant remains an important challenge to physicists and cosmologists [13].

1.1.2 Chameleon Dark Energy

One of the most intriguing discoveries in modern cosmology is the accelerating expansion of the universe. This acceleration is said to be caused by a fluid component of the universe which has negative pressure, this form of energy density is called dark energy

(DE). Cosmological observations such as supernovae luminosity-distance measurements [14], and the cosmic microwave background anisotropy [15] suggests that DE forms about 70% of the energy density of the universe.

A number of solutions to the dark energy problem have been proposed in literature, the simplest is the cosmological constant Λ, but dark energy is more generally modeled as a quintessence scalar field rolling down a flat potential [16]. For the quintessence scalar field to be evolving on cosmological scales to day its mass must be of order $H_0 \sim 10^{-33}$eV, which is the present value of the Hubble constant. Furthermore, measurements of absorption lines in the spectra of quasars may indicate the variations of the fine-structure constant α of order 10^{-5} in the range of redshift between $(0.2 < z < 3.7)$ [17]. The time evolution of coupling constants are modeled with rolling scalar fields [18], recent evidence for the time evolution of α requires that the mass of the scalar field in the model be of order H_0 [19], but this is not conclusive.

Theoretically string and supergravity theories are populated with massless scalar fields or moduli. Generic compactifications of string theory result in plenty of massless scalars in the low-energy four dimensional effective theory. The coupling of these massless fields to matter with gravitational strength lead to undesirable large violations of the Equivalence Principle. Hence, if one of these massless fields are responsible for quintessence or the time-evolving α, there must be some mechanism to suppress it's violation of the EP [1].

A scalar field ϕ whose mass varies with the background energy density was proposed by Khoury and Weltman [1]. This scalar field can evolve cosmologically while having coupling β_i[1] to different matter fields of order unity. On Earth for example, the mass of ϕ is sufficiently large i.e $\mathcal{O}(1\text{mm}^{-1})$, while in the interstellar medium (ISM) its Compton wavelength is typically hundreds of astronomical units(AU). As a result ϕ evades equivalence principle(EP)(related to the equivalence of gravitational and inertial mass of an object) tests and fifth force (In addition to the four known forces and this fifth force is mediated by the Chameleon field) constraints from laboratory experiments. The dependence of this scalar fields mass on its environment has given it the name "chameleon scalar field".

The density dependent mass for the scalar field ϕ is due to two different source terms in its equation of motion. One of the terms arises from self-interactions determined by a runaway potential $V(\phi)$ of the form shown in Figure (1) below

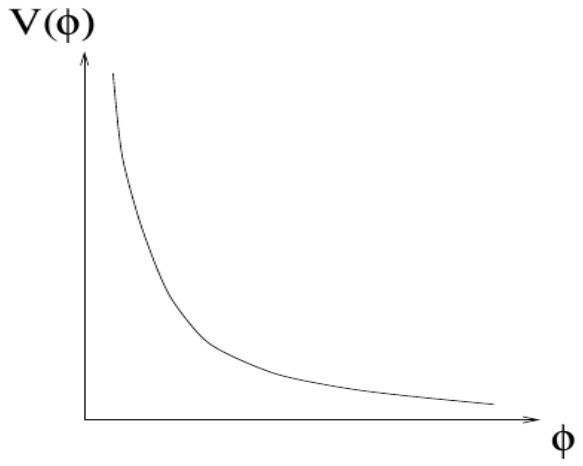

Figure 1: Example of a runaway potential[1, 2].

[1] i labels different matter fields

While the other term comes from the conformal coupling to matter fields of the form $e^{\beta_i \phi / M_{Pl}}$, where the β_is are the coupling constants to different matter fields. Combining these two monotonic functions of ϕ yields an effective potential with a minimum which is depicted in Figure (2) below and depends on the local matter density ρ

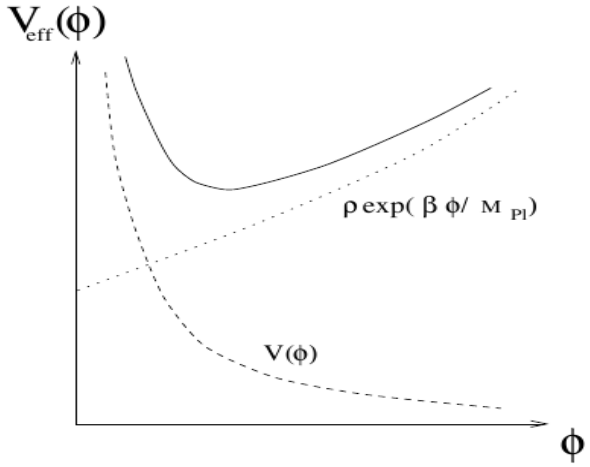

Figure 2: The form of the effective potential for the chameleon field.

As a result the field value and the mass of small fluctuations at this minimum depend on the local matter density, with the mass being an increasing function of the density [1, 2].

To paint a picture of how this works let us consider the general scalar-tensor theory as follows:

$$S = \int d^4x\sqrt{-g}\left\{\frac{M_{Pl}^2}{2}R - \frac{(\partial\phi)^2}{2} - V(\phi) + \mathcal{L}_m(\psi_m, A^2(\phi)g_{\mu\nu})\right\} \tag{1}$$

where ϕ is the chameleon scalar field and $V(\phi)$ is its potential depicted in figure (1), ψ_m are fermion matter fields which couple to the chameleon through $A^2(\phi)$ dependance of the matter Lagrangian $\mathcal{L}_m$ [3]. Therefore the Klein-Gordon equation for the chameleon

scalar field is

$$\nabla^2\phi = V_{,\phi} - \alpha_\phi T^\mu_\mu \tag{2}$$

where $\alpha_\phi = \frac{\partial \ln A}{\partial \phi}$, with the extra term due to the conformal coupling $A^2(\phi)$ and is proportional to the trace of the matter stress-tensor. For a pressure-less (non-relativistic) perfect fluid with density ρ_m that is conserved with respect to the Einstein frame metric $g_{\mu\nu}$, we can approximate this equation (2) by the following equation:

$$\nabla^2\phi = V_{,\phi} - \alpha_\phi \rho_m A(\phi). \tag{3}$$

We can see that the dynamics of the chameleon scalar field are governed by an effective potential V_{eff}, that varies with density ρ_m.

$$V_{eff} = V(\phi) + \rho_m A(\phi) \tag{4}$$

The chameleon couples to matter directly, hence it mediates a "fifth force" which can be experimentally constrained. The magnitude of this force can be suppressed in two ways. Firstly, since the mass of the chameleon field increases with density, the range of the chameleon field can be less than a millimeter in regions of high density (eg. the Earth). This range is short enough to satisfy current bounds from fifth force experiments in the laboratory. Secondly, is the so-called thin-shell mechanism, which means for large enough objects the ϕ-force on a test particle is contributed by a thin shell of matter just underneath the surface of the object. Whereas the matter deep inside the object contributes a negligible amount.

To show how this "thin-shell" mechanism manifest, we consider a solution for the chameleon field in the case of a spherically-symmetric object of radius R and homoge-

neous density ρ. For our purpose we shall focus on the inverse power-law potential of the form $V(\phi) = \frac{M^{4+n}}{\phi^n}$, in which M has mass units and a coupling of the form $A(\phi) = \exp(\beta\phi)$ of gravitational strength (β of order one). At the boundary we want the solution to be non-singular at the origin and ϕ should turn to its background value ϕ_0 at infinity. Within a sufficiently large object, the value of the field is ϕ_c in which the c stands for "core" [3].

The effective potential has a minimum at this value given by this equation: $V_{,\phi}(\phi_c) + \beta\rho_c \exp(\beta\phi_c/M_{Pl})/M_{Pl}$. This condition is valid everywhere inside the object but within a thin shell of matter with thickness ΔR just below the surface where the field value starts to grow. The profile of the chameleon outside the object is that of a scalar field with mass m_0 of the form $\phi \sim \exp(-m_0 r)/r$. The thickness of the shell can be approximated in terms ϕ_0, ϕ_c and the Newtonian potential of the object given by: $\Phi_N = M/8\pi M_{Pl}^2 R$ in the following way;

$$\frac{\Delta R}{R} \approx \frac{\phi_0 - \phi_c}{6\beta M_{Pl}\Phi_N}. \tag{5}$$

The profile for ϕ outside the object can be written explicitly as [1].

$$\phi(r) \approx -\left(\frac{\beta}{4\pi M_{Pl}}\right)\left(\frac{3\Delta R}{R}\right)\frac{Me^{-m_0(r-R)}}{r} + \phi_0 \tag{6}$$

1.2 Chameleon cosmology

Cosmologically, in a homogeneous, isotropic and spatially flat universe described by the Friedmann-Lemaître-Robertson-Walker (FLRW) metric $ds^2 = -dt^2 + a^2(t)d\vec{x}^2$, equation (2) becomes

$$\ddot{\phi} + 3H\dot{\phi} = -V_{,\phi}(\phi) - \frac{\beta}{M_{Pl}}\rho_m e^{\frac{\beta\phi}{M_{Pl}}} \tag{7}$$

with ρ_m being the energy density in the non-relativistic component (dust), and the dot represents the derivative with respect to cosmological time t. In an expanding universe the density of matter redshifts as a^{-3}, where a is the scale factor. This means that the effective potential (V_{eff}) is time dependent. Hence the value of the field ϕ_{min} at the minimum of V_{eff} increases with time, as seen from Figure(1). However, one can show that the mass of ϕ of small fluctuations about the minimum satisfies the condition that $m \gg H$. This means that the chameleon response time m^{-1} is shorter than the time over which the potential evolute H^{-1}. Hence the evolution is adiabatic [3].

When the chameleon starts at the minimum of the effective potential it stays at the minimum as the V_{eff} evolves with time, this is a dynamic attractor. In general, initial conditions fall into undershoot or overshoot solutions, which is similar to their counterparts in the quintessence models. When the chameleon starts at the value $\phi_i \gg \phi_{min}$, this correspond to the undershoot solution. In this case the bare potential ($V(\phi)$) can be neglected, and we have the evolution equation for ϕ as follows;

$$\ddot{\phi} + 3H\dot{\phi} \approx \frac{\beta}{M_{Pl}} T^{\mu}_{\mu}, \tag{8}$$

commonly we can approximate T^{μ}_{μ} to be zero during the radiation dominated era since a relativistic fluid has a trace of zero [3].

In this case the chameleon field will stay at its initial value because of Hubble damping, and will not reach the attractor early enough. However in reality we can not always neglect the trace during the radiation era, because as the universe expands it cools, and different particles species become non-relativistic successively. Hence making the trace

non-zero for about one e-fold of expansion, thus the chameleon is driven to the minimum [3]. Eventually the field is displaced by $|\Delta\phi| \approx \beta M_{Pl}$ see Figure (3).

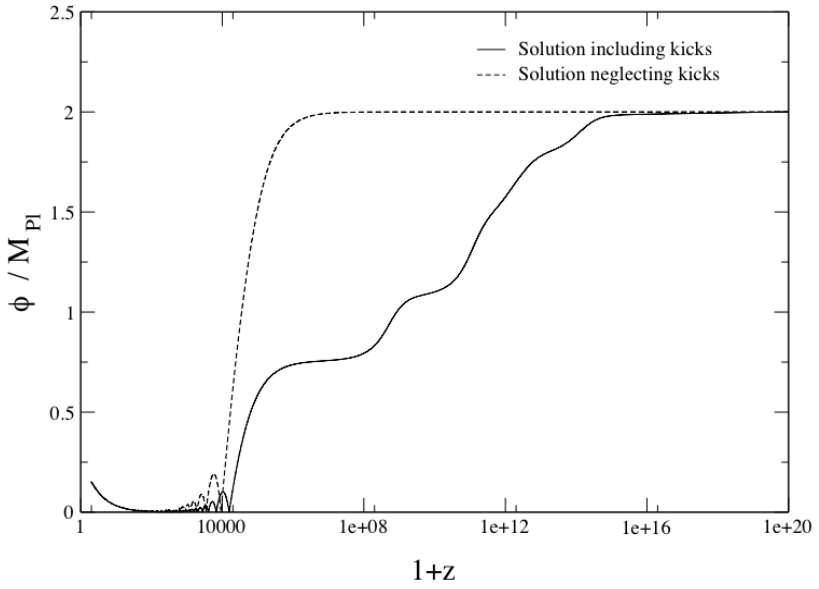

Figure 3: The effect of kicks on the chameleon. Ignoring the kicks (dashed curve), the chameleon remains frozen at its initial value during the radiation era due to Hubble damping. Including the kicks (solid curve), however, results in a total displacement of order M_{Pl} [3].

The chameleon must be at the minimum at the beginning of big bang nucleosynthesis, to prevent causing unacceptable large variations in masses and couplings. This is satisfied as long as $\phi_i \sim M_{Pl}$ for $\beta \sim \mathcal{O}(1)$ where ϕ_i is the initial value of the chameleon. In the case of the overshoot solution, which corresponds to $\phi_i \ll \phi_{min}$. The field starts high up on the potential, due to being kinetic-dominated it overshoots the minimum and it is brought to a stop by the Hubble damping at the value $\phi_{stop} \gg \phi_{min}$.

It can be shown that the latter is given by $\phi_{stop} = \phi_i + \sqrt{6\Omega_\phi^{(i)}} M_{Pl}$, in which $\Omega^{(i)}$ is the initial chameleon fractional energy density. After this the solution follows the undershoot case. The big bang nucleosynthesis(BBN) constraints require that $\phi_{stop} \sim M_{Pl}$, and thus $\Omega_\phi^{(i)} \sim \frac{1}{6}$ which is consistent with equipartition at reheating. Since the chameleon couples to matter, a variation of $\Delta\phi$ gives rise to changes in particle masses by $|\frac{\Delta m}{m}| = \beta \frac{|\Delta\phi|}{M_{Pl}}$.

From BBN until present day, the measured abundance of light elements constrains $|\frac{\Delta m}{m}|$ to be less than about 10%. This means that BBN requires that $|\phi_{BBN} - \phi^{(0)}| \sim 0.1 M_{Pl}$ for $\beta \sim \mathcal{O}(1)$, where ϕ_{BBN} and $\phi^{(0)}$ are the values of the field at BBN and today respectively. It is fortunate that the chameleon at the minimum satisfies $\phi_{min} \ll M_{Pl}$ for all relevant times. Hence this bound is satisfied if ϕ is at the minimum at the beginning of BBN [3].

1.3 Mixing of Chameleons/Axions with photons

When a photon propagates through a region with an external electromagnetic field, it may create a particle with a two-photon vertex. This particle may have a very small mass or no mass at all, causing a near-degeneracy with the photon. Hence a mixing phenomenon is expected between this low-mass particle and the photon, which is similar to the the familiar K^0-meson or neutrino-flavor mixing systems.

The difference between the latter two and the former mixing phenomena is that for the photon and low-mass particle system the superposition of states can contain components with different spins and polarization, because the presence of an external magnetic field

makes the conservation of angular momentum unnecessary. Thus the mixing of photons with spin-0 or spin-2 particles is possible [20].

For this kind of mixing to occur we need to have a transverse external magnetic field to the direction of propagation. Since the transition from a free photon state to a spin-0 particle requires a change in the azimuthal angular momentum quantum number (J_z), the photon and the chameleon (spin-0) particle have $J_z = \pm 1$ and $J_z = 0$ respectively. Therefore a longitudinal magnetic field which gives the problem an azimuthal symmetry does not lead to a change in (J_z), hence no mixing will occur [20].

The chameleon scalar field also couples to photons in the presence of an external magnetic field as described above [20] via the ϕF^2 interaction term, where F stands for the electromagnetic field strength tensor . The chameleon-photon coupling of this nature causes a conversion of photons to light chameleon particles and vice versa. These effects are similar to those of Axion-like particles(ALPs) which interact with light [21].

1.4 Chameleon Laboratory searches

1.4.1 The GammeV Experiment

The GammeV experiment was a quantum vacuum experiment conducted at Fermilab. This experiment was intended to probe the coupling of chameleons to photons through the electromagnetic interaction with the external magnetic field. The set up is as follows, consider a vacuum chamber with walls of density ρ_{wall}, these walls must be thicker than the chameleon Compton wavelength at this density.

Inside the chamber the chameleons are almost massless and they will not be affected by the chameleon field inside the wall. As the chameleon approaches the wall its mass will increase and it will bounce elastically off the wall if its momentum is less than the chameleon mass inside the wall. In this sense the vacuum chamber will be a container for the chameleon particles.

When shining light through the vacuum chamber the photons will interact with the magnetic field and will oscillate into chameleon particles. When the chameleon and photon superposition of states hits the glass window at the side of the vacuum chamber, the photons will pass through the glass while the chameleons get reflected. So continually supplying photons inside the chamber will increase the number of chameleon particles.

When the supply of photons is stopped, chameleons will convert back into photons which will exit the chamber through the glass window. Thus the GammeV experiment looks for this "Afterglow" effect, The schematic of this experiments apparatus can be seen in figure (4) [4].

1.4.2 The CHASE laboratory search for chameleon dark energy

The Chameleon Afterglow Search (CHASE) experiment is a version of the GammeV experiment discussed in the previous section. Its results bridge the gap between GammeV and collider constrains, and improves sensitivity to the photon couplings to chameleons. The results of this experiment revealed no evidence for a photon-coupled chameleon. The

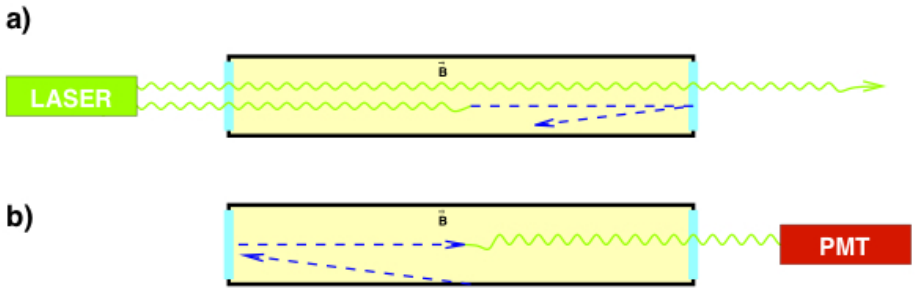

Figure 4: Schematic of the GammeV apparatus. a) Chameleon production phase: photons propagating through a region of magnetic field oscillate into chameleons. Photons travel through the glass end caps whereas chameleons see the glass as a wall and are trapped. b) Afterglow phase: chameleons in the chamber gradually decay back into photons and are detected by a photomultiplier tube.[4].

constraints reach four significant milestones.

Firstly, they bridge the three orders of magnitude gap between bounds on β_γ from the GammeV and from colliders. Secondly, they exclude a range of β_γ covering four orders of magnitude at masses similar to the dark energy scale ($2.4 \times 10^{-3} eV$). Thirdly, they rule out photon-chameleon couplings in the range $\beta_\gamma < 7.1 \times 10^{10}$ for scalar and $\beta_\gamma < 7.6 \times 10^{10}$ for pseudo-scalar chameleons [5], but these constraints are sensitive to chameleon dark energy models.

These constraints complement those from the torsion pendular, which probe $\beta_m \sim 1$, and are consistent with those from Casimir force experiments. Data form the CHASE experiment exclude chameleon to photon coupling spanning five orders of magnitude, and they exclude over twelve orders of magnitude in chameleon to matter coupling for

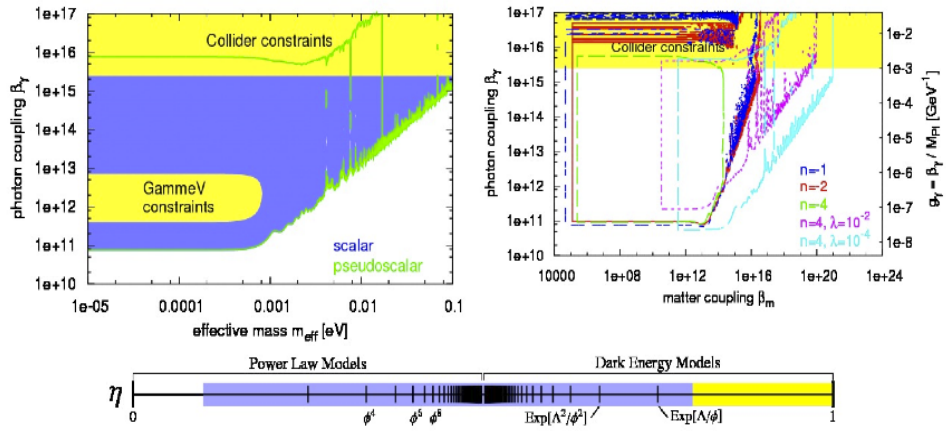

Figure 5: Left: Scalar (solid) and pseudo-scalar (outline) constraints, at 95% confidence, in the (m_{eff},β_γ) plane. Right: 95% confidence-level constraints on chameleons with power law potentials. Bottom: Chameleon models probed by CHASE. GammeV sensitivity is yellow while CHASE sensitivity is blue.[5]

individual models.

1.5 Chameleon Astrophysical Searches

1.5.1 Chameleon-photon Mixing in the Supernova

There will be a chameleon particle flux emitted by the supernova explosion if some of the photons produced by the explosion are converted into chameleons inside the supernova with a certain probability. In order to calculate the chameleon-photon mixing probability inside the supernova, consider a toy model outlined by [22], where the supernova is assumed to be a sphere with uniform density and an initial radius of approximately 10^9cm. It expands with velocity $v = \frac{c}{30} \sim 10^9$cm/s where c is the speed of light.

And we also assume for simplicity that the length of the magnetic domain in the supernova is approximately the same as the photon mean free path and that the explosion only produces photons and are emitted uniformly throughout the volume of the supernova. Supernova explosions are homologous, thus the magnetic field satisfies the following condition $\frac{B_{SN}(t)}{B_{WD}} = \left(\frac{R_{WD}}{R_{SN}(t)}\right)^2$ where $B_{SN}(t)$ and R_{SN} are the magnetic field and radius of the supernova at some time t following the explosion, B_{WD} and R_{WD} are the magnetic field and radius of the white dwarf progenitor.

When the supernova reaches its peak luminosity the photon mean free path can be modelled as a random walk such that photons take $N = 3R^2/L_{mfp}^2$ steps to escape from the volume with radius R where L_{mfp} denotes the photon mean free path. Therefore the probability of a photon converting into a chameleon inside the supernova is

$$P_{\gamma\to\phi}(R_{SN}) \lesssim \frac{3B_{SN}^2 R_{SN}^2}{8M^2} \tag{9}$$

where $M = \frac{\beta_\gamma}{M_{Pl}}$, β_γ is the chameleon-photon coupling constant and M_{Pl} is the Planck mass. Even though only photons are emitted by the thermonuclear reactions in the supernova, this probability indicates that there is a significant flux of chameleons at the surface of the supernova as a result of photons being converted to chameleons.

If there is a chameleon particle flux at the surface of the supernova and the photon number is not conserved in the intergalactic medium then relation between luminosity distance and the angular diameter distance given by $d_L = d_A(z)(1+z)^2$, in which d_L, d_A and z are the luminosity distance, angular diameter distance and the redshift respectively, thus d_L must be changed by the following transformation $d_L \longrightarrow \frac{d_L}{\sqrt{P_{\gamma\to\phi}}}$. Due to

the strong magnetic field inside a supernova, the is a chameleon-photon mixing inside the supernova which will lead to a flux of chameleon particles at the surface of the supernova.

Feather more, chameleons and photons mix as they propagate through the intergalactic magnetic fields, which requires $M \lesssim 10^{10}\text{GeV}$ to ensure that the effect of the mixing is achromatic for optical photons. The photon-chameleon coupling of this strength should be detectable with future experiments which looks for this chameleonic afterglow phenomenon [23, 24] or Casimir forces. The effect of this mixing results in the brightening of supernovae, which shows that something is causing the discrepancy between the observations of standard candles and standard rulers. We wait for the future observations of distant supernova to improve the constrains on this model [22].

1.6 Astronomical Polarization Produced by Chameleon Scalar Fields

1.6.1 Chameleon-Photon Optics

When photons propagate through a region of space with a background magnetic field, the presence of the chameleon field alters the properties of light through the process of chameleon-photon oscillations. If photons propagate through a region with electron number density n_e, they behave as if they have an effective mass ω_p where $\omega_p^2 = 4\pi\alpha n_e/m_e$ is the plasma frequency, α is the fine structure constant and m_e is the electron mass [21].

In the chameleon model the component of the photon field that couples to the chameleon field is one that is polarized perpendicular to the background magnetic field,

with the other polarization propagating freely. From the evolution amplitudes of the two polarizations we can define the observable Stokes parameters as follows:

$$I_\gamma = \langle|\gamma_\parallel|^2\rangle + \langle|\gamma_\perp|^2\rangle \tag{10}$$

$$Q = \langle|\gamma_\parallel|^2\rangle - \langle|\gamma_\perp|^2\rangle \tag{11}$$

$$U + iV = 2\langle\overline{\gamma}_\perp\gamma_\parallel\rangle \tag{12}$$

where we have defined $\gamma_\perp$ and $\gamma_\parallel$ to be the components of the photon field perpendicular and parallel to the external magnetic field, therefore the Stokes vector for the photon field is given by $S = [I_\gamma, Q, U, V]^T$. V describes the amount of circular polarization, Q and U both describes the amount of linear polarization. The reduced Stokes vector is $S_{red} = [Q/I_\gamma, U/I_\gamma, V/I_\gamma]^T$ and the fraction of light that is polarized is:

$$p = \sqrt{\frac{Q^2 + U^2 + V^2}{I_\gamma}} \tag{13}$$

If chameleon particles are coupled to photons then they will mix with the component of the photon polarization that is orthogonal to the magnetic fields alignment in the background. Thus usually this type of mixing will cause both linear and circular polarization in the beam of light. If the light is not polarized at the source when emitted the averages of the circular and the total polarization scale as $NP_{\gamma\leftrightarrow\phi}$, where N is the number of magnetic domains and $P_{\gamma\leftrightarrow\phi}$ is the probability of mixing in any of the domains [21].

In the strong mixing limit little or no circular polarization is produced by the mixing, but the production of linear polarization is at its strongest. The distribution of the total polarization fraction after mixing over a large number magnetic domains is independent of the parameters of the chameleon model, it only depend on the initial polarization of

the light. In the maximum mixing limit the average value of the total polarization is greater than $\pi/2 - 1 \approx 0.57$ [21].

Observations of starlight in the Galaxy show at 99% confidence level $M > 1.1 \times 10^9 GeV$, where $M = M_{Pl}/\beta_\gamma$ in which M_{Pl} is the Planck mass and β_γ is the chameleon-photon coupling constant. This constraint on M is an improvement of two orders of magnitude on the previous best constraints. Constrains from extragalactic objects are limited by the poor knowledge of intergalactic magnetic fields. A strong statistical preference in observations of starlight polarization in the Galaxy for the presence of a chameleon field was reported, at the 99% confidence level, it was found that

$$\left(\frac{|B|L}{2M}\right)_{rand} = (6.27 \pm 1.91) \times 10^{-2} \tag{14}$$

where B and L are the strength and domain size of the random component of the galactic magnetic field [21].

1.7 Overview

The layout of this document is organised in the following way, section 2 we discuss chameleon scalar field phenomenology, where we provide the basic equations motion for the chameleon and photon fields and the chameleon effective mass, in section 3 we discuss chameleon-photon mixing mechanism, section 4 is the search for chameleon-photon mixing in pulsars, section 5 is the results section followed by the discussion section 6, section 7 and 8 are the conclusions and recommendations respectively.

2 Chameleon phenomenology

2.1 Chameleon Action

We consider the following chameleon action S adapted from [25],

$$S = \int d^4x\sqrt{-g}\left(\frac{1}{2}M_{Pl}^2R - \frac{1}{2}\partial_\mu\phi\partial^\mu\phi - V(\phi) - \frac{e^{\beta_\gamma\phi/M_{Pl}}}{4}F^{\mu\nu}F_{\mu\nu}\right) + \int d^4x\left(\mathcal{L}_m(e^{2\beta_m\phi/M_{Pl}}g_{\mu\nu}, \psi_m^{(i)})\right) \tag{15}$$

where S is the sum of the normalized vacuum Einstein-Hilbert action(S_{EH}) by equation (16), in which R is the Ricci scalar, $M_{Pl} = (8\pi G)^{-1/2}$ is the reduced Planck mass and g is the determinant of the metric tensor $g_{\mu\nu}$ [26].

$$S_{EH} = \int dx^4\sqrt{-g}\frac{1}{2}M_{Pl}^2R, \tag{16}$$

The second and the third terms give the scalar field ϕ action, with a potential $V(\phi)$ which is of a runaway form depicted in figure(1), the potential of this form is required to have the following characteristics given in [1].

$$\lim_{\phi\to+\infty} V(\phi) = 0, \quad \lim_{\phi\to+\infty}\frac{V_{,\phi}}{V} = 0, \quad \lim_{\phi\to+\infty}\frac{V_{,\phi\phi}}{V_{,\phi}} = 0...,$$

as well as

$$\lim_{\phi\to0} V(\phi) = \infty, \quad \lim_{\phi\to0}\frac{V_{,\phi}}{V} = \infty, \quad \lim_{\phi\to0}\frac{V_{,\phi\phi}}{V_{,\phi}} = \infty...,$$

The scalar field action is as follows,

$$S_\phi = \int dx^4\sqrt{-g}\left(-\frac{1}{2}\partial_\mu\phi\partial^\mu\phi - V(\phi)\right), \tag{17}$$

and finally we have

$$\mathcal{L}_\gamma = -\frac{e^{\beta_\gamma\phi/M_{Pl}}}{4}F^{\mu\nu}F_{\mu\nu}, \tag{18}$$

and

$$\mathcal{L}_m(e^{2\beta_m\phi/M_{Pl}}g_{\mu\nu}, \psi_m^{(i)}) \tag{19}$$

which are the photon-scalar and matter-scalar interaction Lagrangians respectively. The $\psi_m^{(i)}$ are matter fields which couple to ϕ by a conformal coupling of the form $g_{\mu\nu}^{(i)} = e^{2\beta_m\phi/M_{Pl}}g_{\mu\nu}$ [1], in which β_m and β_γ are dimensionless matter-chameleon and photon-chameleon coupling constants respectively.

2.2 Equation of Motion for ϕ

To obtain the equation of motion for ϕ we vary the action S with respect to ϕ, and using that $g_{\mu\nu}^i = e^{2\beta_m\phi/M_{Pl}}g_{\mu\nu}$.

$$\begin{aligned}\delta S &= \int d^4x\sqrt{-g}\left(-\frac{1}{2}[\partial_\mu\delta\phi\partial^\mu\phi + \partial_\mu\phi\partial^\mu\delta\phi] - V_{,\phi}(\phi)\delta\phi - \frac{\beta_\gamma e^{\beta_\gamma\phi/M_{Pl}}}{4M_{Pl}}F^{\mu\nu}F_{\mu\nu}\delta\phi\right) \\ &\quad + \int d^4x\left(\frac{\partial\mathcal{L}_m}{\partial\phi}\delta\phi\right) \qquad (20) \\ &= \int d^4x\sqrt{-g}\left(-\partial_\mu\phi\partial^\mu\delta\phi - V_{,\phi}(\phi)\delta\phi - \frac{\beta_\gamma e^{\beta_\gamma\phi/M_{Pl}}}{4M_{Pl}}F^{\mu\nu}F_{\mu\nu}\delta\phi + \frac{\delta\phi}{\sqrt{-g}}\frac{\partial\mathcal{L}_m}{\partial g_{\mu\nu}^i}\frac{\partial g_{\mu\nu}^i}{\partial\phi}\right) \\ &= \int d^4x\sqrt{-g}\left((\partial_\mu\partial^\mu\phi)\delta\phi - V_{,\phi}(\phi)\delta\phi - \frac{\beta_\gamma e^{\beta_\gamma\phi/M_{Pl}}}{4M_{Pl}}F^{\mu\nu}F_{\mu\nu}\delta\phi\right) \\ &\quad + \int d^4x\left(\frac{2\beta_m}{M_{Pl}}\frac{\partial\mathcal{L}_m}{\partial g_{\mu\nu}^i}e^{2\beta_m\phi/M_{Pl}}g_{\mu\nu}\delta\phi\right) \qquad (21)\end{aligned}$$

We require that $\delta S = 0$ in order to obtain the equation of motion for ϕ, therefore

$$\partial_\mu\partial^\mu\phi - V_{,\phi}(\phi) - \frac{\beta_\gamma e^{\beta_\gamma\phi/M_{Pl}}}{4M_{Pl}}F^{\mu\nu}F_{\mu\nu} + \frac{2\beta_m}{M_{Pl}\sqrt{-g}}\frac{\partial\mathcal{L}_m}{\partial g_{\mu\nu}^i}e^{2\beta_m\phi/M_{Pl}}g_{\mu\nu} = 0 \tag{22}$$

For dust, we find in the Jordan frame the energy-momentum tensor from [1] $\tilde{T}^{\mu\nu} \equiv -\frac{2}{\sqrt{-\tilde{g}}}\frac{\partial\mathcal{L}_m}{\partial\tilde{g}_{\mu\nu}}$ where $\tilde{\nabla}_\nu\tilde{T}^{\mu\nu} = 0$ and we define $\rho_m = e^{\beta_m\phi/M_{Pl}}\tilde{\rho}$. Therefore $\tilde{T}^{\mu\nu}\tilde{g}_{\mu\nu} = -\tilde{\rho}$, which gives the following equation of motion.

$$\Box\phi = V_{,\phi}(\phi) + \frac{\beta_\gamma e^{\beta_\gamma\phi/M_{Pl}}}{4M_{Pl}}F^{\mu\nu}F_{\mu\nu} + \frac{\beta_m}{M_{Pl}}e^{\beta_m\phi/M_{Pl}}\rho_m \tag{23}$$

Equation (23) can be written in a Klein-Gordon form as follows

$$\Box\phi = -\frac{\partial V_{eff}}{\partial \phi} \tag{24}$$

where V_{eff} is the effective chameleon potential shown below and its form is shown in figure (2).

$$V_{eff}(\vec{x}, \phi) = V(\phi) + e^{\frac{\beta_m \phi}{M_{Pl}}}\rho_m + e^{\frac{\beta_\gamma \phi}{M_{Pl}}}\rho_\gamma \tag{25}$$

in which $\rho_\gamma = (F^{\mu\nu}F_{\mu\nu})/4 = (|\vec{B}|^2 - |\vec{E}|^2)/2$ is the electromagnetic field Lagrangian density, and ρ_m is the matter density. We assume the fiducial exponential potential used in chameleon dark energy theories given by the following equation [25] and $\kappa > 0$.

$$V(\phi) = M_\Lambda^4 \exp\left[\kappa\left(\frac{M_\Lambda}{\phi}\right)^n\right] \tag{26}$$

which we can approximate by an inverse power law potential if we assume that $M_\Lambda/\phi \ll 1$.

$$V(\phi) \approx M_\Lambda^4\left[1 + \kappa\left(\frac{M_\Lambda}{\phi}\right)^n\right] \tag{27}$$

2.3 Chameleon Effective Mass

The effective mass of small fluctuations about the minimum of V_{eff} in figure(2) is given by equation (28) bellow

$$m_{eff}^2(\phi) = \frac{\partial^2 V_{eff}}{\partial \phi^2} \tag{28}$$

$$= n(n+1)\kappa\frac{M_\Lambda^{n+4}}{\phi^{n+2}} + \frac{\beta_m^2\rho_m}{M_{Pl}^2}e^{\frac{\beta_m\phi}{M_{Pl}}} + \frac{\beta_\gamma^2\rho_\gamma}{M_{Pl}^2}e^{\frac{\beta_\gamma\phi}{M_{Pl}}} \tag{29}$$

$$m_{eff}^2(\phi_{min}) = n(n+1)\kappa\frac{M_\Lambda^{n+4}}{\phi_{min}^{n+2}} + \frac{\beta_m^2\rho_m}{M_{Pl}^2} + \frac{\beta_\gamma^2\rho_\gamma}{M_{Pl}^2} \tag{30}$$

where ϕ_{min} is the value of ϕ at the minimum value of the effective potential, which can be calculated as follows

$$\frac{\partial V_{eff}}{\partial \phi} = 0 \tag{31}$$

$$V_{,\phi}(\phi_{min}) + \frac{\beta_m \rho_m}{M_{Pl}} e^{\frac{\beta_m \phi}{M_{Pl}}} + \frac{\beta_\gamma \rho_\gamma}{M_{Pl}} e^{\frac{\beta_\gamma \phi}{M_{Pl}}} = 0 \tag{32}$$

$$-n\kappa \frac{M_\Lambda^{n+4}}{\phi_{min}^{n+1}} + \frac{\beta_m \rho_m}{M_{Pl}} + \frac{\beta_\gamma \rho_\gamma}{M_{Pl}} = 0 \tag{33}$$

hence

$$\phi_{min} = \left(\frac{n\kappa M_\Lambda^{n+4} M_{Pl}}{\beta_m \rho_m + \beta_\gamma \rho_\gamma} \right)^{\frac{1}{n+1}}. \tag{34}$$

Therefore substituting equation(34) into (30) we get the following

$$m_{eff}(\phi_{min}) = \sqrt{n(n+1)\kappa^{-\left(\frac{1}{n+1}\right)} M_\Lambda^{n+4} \left(\frac{\beta_m \rho_m + \beta_\gamma \rho_\gamma}{n M_\Lambda^{n+4} M_{Pl}} \right)^{\frac{n+2}{n+1}} + \frac{\beta_m^2 \rho_m}{M_{Pl}^2} + \frac{\beta_\gamma^2 \rho_\gamma}{M_{Pl}^2}}. \tag{35}$$

In equation (30) and (33) we assumed that $\phi/M_{Pl} \ll 1$, hence $e^{\frac{\beta_m \phi}{M_{Pl}}}$ and $e^{\frac{\beta_\gamma \phi}{M_{Pl}}}$ are both approximately equal to one. Looking at the effective mass of the chameleon in equation(35) one can see that it is directly proportional to the local matter density ρ_m and the magnetic energy density, this dependence on energy density is reflected in figure(6) below.

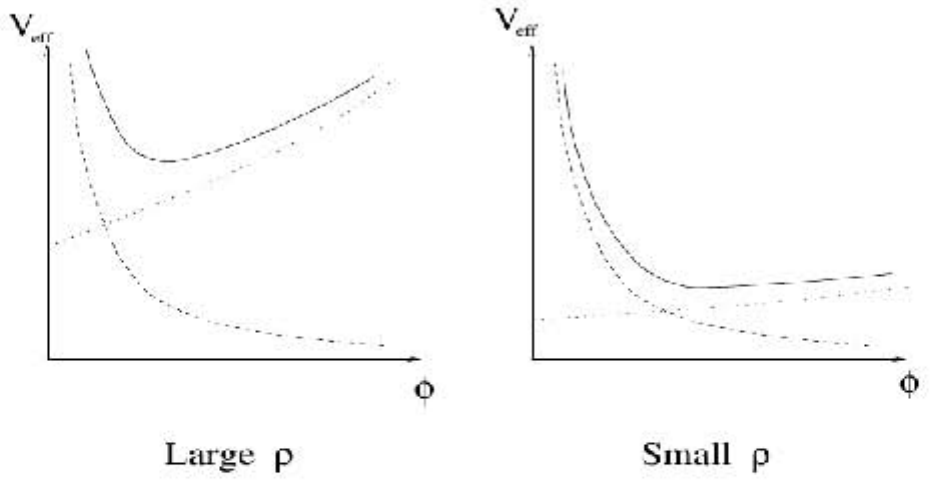

Figure 6: This simple plot shows(left hand side) that in high density regions the value of ϕ is small and the mass is Large. On the right hand side it is shown that in lower density regions the ϕ value is higher and the mass is smaller.

2.4 Equation of motion for the photon field

We vary the action in (15) with respect to A^μ which is the electromagnetic 4-potential, $\eta_{\mu\nu}$ is the Minkowski metric with signature $\{-+++\}$.

$$\delta S = \int d^4x\sqrt{-g}\left(-\frac{1}{4}e^{\beta_\gamma\phi/M_{Pl}}\eta_{\mu\lambda}\eta_{\nu\rho}[\delta F^{\mu\nu}F^{\lambda\rho}+F^{\mu\nu}\delta F^{\lambda\rho}]\right) \tag{36}$$

$$= \int d^4x\sqrt{-g}\left(-\frac{1}{2}e^{\beta_\gamma\phi/M_{Pl}}\eta_{\mu\lambda}\eta_{\nu\rho}\delta F^{\mu\nu}F^{\lambda\rho}\right) \tag{37}$$

$$= \int d^4x\sqrt{-g}\left(-\frac{1}{2}e^{\beta_\gamma\phi/M_{Pl}}\delta F_{\lambda\rho}F^{\lambda\rho}\right) \tag{38}$$

$$= \int d^4x\sqrt{-g}\left(-\frac{1}{2}e^{\beta_\gamma\phi/M_{Pl}}[\partial_\lambda\delta A_\rho-\partial_\rho\delta A_\lambda]F^{\lambda\rho}\right) \tag{39}$$

$$= \int d^4x\sqrt{-g}\left(-e^{\beta_\gamma\phi/M_{Pl}}\partial_\lambda\delta A_\rho F^{\lambda\rho}\right) \tag{40}$$

$$= \int d^4x\sqrt{-g}\left(\delta A_\rho\partial_\lambda(e^{\beta_\gamma\phi/M_{Pl}}F^{\lambda\rho})\right) \tag{41}$$

again we require that the $\delta S = 0$ we obtain the equation of motion as

$$\partial_\lambda(e^{\beta_\gamma \phi/M_{Pl}} F^{\lambda\rho}) = 0 \tag{42}$$

$$\partial_\lambda(e^{\beta_\gamma \phi/M_{Pl}}[\partial^\lambda A^\rho - \partial^\rho A^\lambda]) = 0$$

$$\partial_\lambda \phi \frac{\beta_\gamma}{M_{Pl}} e^{\beta_\gamma \phi/M_{Pl}}[\partial^\lambda A^\rho - \partial^\rho A^\lambda] + e^{\beta_\gamma \phi/M_{Pl}}[\partial_\lambda \partial^\lambda A^\rho - \partial_\lambda \partial^\rho A^\lambda] = 0$$

using the rotation gauge $\partial_\mu \partial^\nu A^\mu = \partial_\nu \partial^\mu A^\mu = 0$ and dividing by $e^{\beta_\gamma \phi/M_{Pl}}$ we get

$$\frac{\beta_\gamma}{M_{Pl}} \partial_\lambda \phi[\partial^\lambda A^\rho - \partial^\rho A^\lambda] + \partial_\lambda \partial^\lambda A^\rho = 0 \tag{43}$$

thus it can be shown that (where $A^\mu = (\psi, \vec{A})$ [25]) for the component of the magnetic field interacting with ϕ is given by

$$\frac{\beta_\gamma}{M_{Pl}} \partial_i \phi[\partial^i A^j - \partial^j A^i] + \partial_\lambda \partial^\lambda A^\rho = 0 \tag{44}$$

with (i and j $= 1, 2, 3$, and $(x^1, x^2, x^3) = (x, y, z)$), this gives the following equation in vector form.

$$\frac{\beta_\gamma}{M_{Pl}} \vec{\nabla}\phi \times (\vec{\nabla} \times \vec{A}) + \Box \vec{A} = 0. \tag{45}$$

In equation (45) we have used the following identity

$$\begin{aligned} \vec{\nabla}\phi \times (\vec{\nabla} \times \vec{A}) = &\{\partial_y \phi(\partial_x A_y - \partial_y A_x) + \partial_z \phi(\partial_x A_z - \partial_z A_x)\}\hat{x} \\ &- \{\partial_x \phi(\partial_x A_y - \partial_y A_x) - \partial_z \phi(\partial_y A_z - \partial_z A_y)\}\hat{y} \\ &+ \{\partial_x \phi(\partial_z A_x - \partial_x A_z) + \partial_y \phi(\partial_z A_y - \partial_y A_z)\}\hat{z} \end{aligned} \tag{46}$$

3 Chameleon-photon mixing

3.1 Mixing Matrix Formalism for Calculating $P_{\gamma\leftrightarrow\phi}$

The Chameleon-Photon mixing Probability ($P_{\gamma\leftrightarrow\phi}$) is derived by considering the Chameleon-Photon system shown below, which is obtained from a paper by Raffelt and Stodolsky (1988) [20], where B is the magnetic field strength, ω is the energy, ω_p is the electron plasma frequency of the medium, m_ϕ is the chameleon mass and z is the direction of propagation. The photon and the chameleon fields are indicated by $\vec{\Psi}_\gamma$ and Ψ_ϕ respectively. The photon-chameleon coupling factor is given by $\frac{1}{M} = \frac{\beta_\gamma}{M_{Pl}}$.

$$\left[\omega^2 + \partial_z^2 + \begin{pmatrix} -\omega_p^2 & \frac{B\omega}{M} \\ \frac{B\omega}{M} & -m_\phi^2 \end{pmatrix}\right] \begin{bmatrix} \vec{\Psi}_\gamma \\ \Psi_\phi \end{bmatrix} = 0 \tag{47}$$

In the relativistic limit we have that the dispersion relation is $k \approx \omega$ where $k = \pm\sqrt{\omega^2 - m^2}$ and m stands for ω_p or m_ϕ, since in general we have that $\omega \gg \omega_p$ and m_ϕ, this gives

$$\begin{aligned}(\omega^2 + \partial_z^2) &= (\omega + i\partial_z)(\omega - i\partial_z) \\ &\approx (\omega + k)(\omega - i\partial_z) \\ &\approx 2\omega(\omega - i\partial_z)\end{aligned} \tag{48}$$

In light of this approximation equation (47) becomes

$$\left[\omega - i\partial_z + \begin{pmatrix} -\frac{\omega_p^2}{2\omega} & \frac{B}{2M} \\ \frac{B}{2M} & -\frac{m_\phi^2}{2\omega} \end{pmatrix}\right] \begin{bmatrix} \vec{\Psi}_\gamma \\ \Psi_\phi \end{bmatrix} = 0 \tag{49}$$

where the mixing matrix is given by

$$A = \begin{pmatrix} \Delta_\gamma & \Delta_M \\ \Delta_M & \Delta_\phi \end{pmatrix} \tag{50}$$

with $\Delta_\gamma = -\frac{\omega_p^2}{2\omega}$, $\Delta_M = \frac{B}{2M}$ and $\Delta_\phi = -\frac{m_\phi^2}{2\omega}$. Therefore A can be diagonalized by a rotation matrix

$$P = \begin{pmatrix} \cos\theta & \sin\theta \\ -\sin\theta & \cos\theta \end{pmatrix}, \tag{51}$$

which is the rotation to the primed fields

$$\begin{bmatrix} \vec{\Psi}'_\gamma \\ \Psi'_\phi \end{bmatrix} = \begin{pmatrix} \cos\theta & \sin\theta \\ -\sin\theta & \cos\theta \end{pmatrix} \begin{bmatrix} \vec{\Psi}_\gamma \\ \Psi_\phi \end{bmatrix}, \tag{52}$$

such that $A = PDP^{-1}$, with

$$D = \begin{pmatrix} \lambda_+ & 0 \\ 0 & \lambda_- \end{pmatrix}, \tag{53}$$

where $\lambda_\pm$ are the eigenvalues of the matrix A given by $\lambda_\pm = \frac{\Delta_\gamma+\Delta_\phi}{2} \pm \frac{\sqrt{(\Delta_\gamma-\Delta_\phi)^2+4\Delta_M^2}}{2} = \Lambda \pm \Omega$. In which

$$\Lambda = \frac{\Delta_\gamma + \Delta_\phi}{2}$$
$$\Omega = \frac{\sqrt{(\Delta_\gamma - \Delta_\phi)^2 + 4\Delta_M^2}}{2}.$$

Now we consider a beam of frequency ω in the primed(interacting) fields travelling in the $z-$direction of the following form:

$$\begin{bmatrix} \vec{\Psi}'_\gamma(z,t) \\ \Psi'_\phi(z,t) \end{bmatrix} = \begin{pmatrix} e^{i(\omega t-(\omega+\Lambda+\Omega)z)} & 0 \\ 0 & e^{i(\omega t-(\omega+\Lambda-\Omega)z)} \end{pmatrix} \begin{bmatrix} \vec{\Psi}'_\gamma(0,t) \\ \Psi'_\phi(0,t) \end{bmatrix} \tag{54}$$

by virtue of equation (52), equation (54) becomes

$$P \begin{bmatrix} \vec{\Psi}_\gamma(z,t) \\ \Psi_\phi(z,t) \end{bmatrix} = e^{-i\omega(z-t)} e^{-iDz} P \begin{bmatrix} \vec{\Psi}_\gamma(0,t) \\ \Psi_\phi(0,t) \end{bmatrix} \tag{55}$$

$$\begin{bmatrix} \vec{\Psi}_\gamma(z,t) \\ \Psi_\phi(z,t) \end{bmatrix} = P^{-1} e^{-i\omega(z-t)} e^{-iDz} P \begin{bmatrix} \vec{\Psi}_\gamma(0,t) \\ \Psi_\phi(0,t) \end{bmatrix} \tag{56}$$

We let the transfer matrix $\mathcal{T}(z,t)$ which describes the chameleon-photon interaction(mixing) over a distance z be calculated as follows;

$$\begin{aligned}
\mathcal{T}(z,t) &= P^{-1}e^{-i\omega(z-t)}e^{-iDz}P \\
&= \begin{pmatrix} \cos\theta & -\sin\theta \\ \sin\theta & \cos\theta \end{pmatrix} \begin{pmatrix} e^{i(\omega t-(\omega+\Lambda+\Omega)z)} & 0 \\ 0 & e^{i(\omega t-(\omega+\Lambda-\Omega)z)} \end{pmatrix} \begin{pmatrix} \cos\theta & \sin\theta \\ -\sin\theta & \cos\theta \end{pmatrix} \\
&= e^{-i(\omega(z-t)+\Lambda z)} \begin{pmatrix} [e^{-i\Omega z}\cos^2\theta + e^{i\Omega z}\sin^2\theta] & \cos\theta\sin\theta[e^{-i\Omega z} - e^{i\Omega z}] \\ \cos\theta\sin\theta[e^{-i\Omega z} - e^{i\Omega z}] & [e^{-i\Omega z}\sin^2\theta + e^{i\Omega z}\cos^2\theta] \end{pmatrix} \\
&= e^{-i(\omega(z-t)+\Lambda z)} \begin{pmatrix} [e^{-i\Omega z}\cos^2\theta + e^{i\Omega z}\sin^2\theta] & -i\sin 2\theta\sin\Omega z \\ -i\sin 2\theta\sin\Omega z & [e^{-i\Omega z}\sin^2\theta + e^{i\Omega z}\cos^2\theta] \end{pmatrix} \qquad (57)
\end{aligned}$$

To find θ we note that the strength of the mixing is given the ratio of the off diagonal term to the difference of the diagonal terms in the following way

$$\begin{aligned}
\frac{\Delta_M}{\Delta_\gamma - \Delta_\phi} &= \frac{-i\sin 2\theta\sin\Omega z}{\cos 2\theta[e^{-i\Omega z} - e^{i\Omega z}]} \\
&= \frac{-i\sin 2\theta}{-2i\cos 2\theta} \\
&= \frac{1}{2}\tan 2\theta \qquad (58)
\end{aligned}$$

Therefore it follows that $4\Delta_M^2 = \tan^2 2\theta(\Delta_\gamma - \Delta_\phi)^2$ hence $\Omega = \frac{\sqrt{(\Delta_\gamma-\Delta_\phi)^2+4\Delta_M^2}}{2}$ can be written as

$$\begin{aligned}
\Omega &= \frac{\sqrt{(\Delta_\gamma - \Delta_\phi)^2 + \tan^2 2\theta(\Delta_\gamma - \Delta_\phi)^2}}{2} \\
&= \frac{\sqrt{(\Delta_\gamma - \Delta_\phi)^2(\cos^2 2\theta + \sin^2 2\theta)}}{2\cos 2\theta} \\
&= \frac{\Delta_\gamma - \Delta_\phi}{2\cos 2\theta} \qquad (59)
\end{aligned}$$

Finally the Photon-Chameleon mixing amplitude is given by the off-diagonal terms in $\mathcal{T}(z,t)$, which is $\mathcal{T}_{12}(z,t) = -ie^{-i\omega(z-t)+\Lambda z)} \sin 2\theta \sin \Omega z$ therefore the probability is given by

$$P_{\gamma\leftrightarrow\phi} = |\mathcal{T}_{12}(z,t)|^2 = \sin^2 2\theta \sin^2(\Omega z) \tag{60}$$

$$= \sin^2 2\theta \sin^2\left(\frac{\Delta_\gamma - \Delta_\phi}{2\cos 2\theta} z\right)$$

$$= \sin^2 2\theta \sin^2\left(\frac{\Delta}{\cos 2\theta}\right) \tag{61}$$

where $\Delta = \frac{\Delta_\gamma - \Delta_\phi}{2} z$. For computational purposes we need to express this probability in terms of observables quantities which are the components of matrix A. Noting that

$$\cos 2\theta = \frac{\Delta_\gamma - \Delta_\phi}{\sqrt{(\Delta_\gamma - \Delta_\phi)^2 + 4\Delta_M^2}} \tag{62}$$

therefore

$$\sin^2 2\theta = 1 - \frac{(\Delta_\gamma - \Delta_\phi)^2}{(\Delta_\gamma - \Delta_\phi)^2 + 4\Delta_M^2}$$

$$= \frac{4\Delta_M^2}{(\Delta_\gamma - \Delta_\phi)^2 + 4\Delta_M^2} \tag{63}$$

then the probability becomes,

$$P_{\gamma\leftrightarrow\phi} = \frac{4\Delta_M^2}{(\Delta_\gamma - \Delta_\phi)^2 + 4\Delta_M^2} \sin^2\left(\frac{\sqrt{(\Delta_\gamma - \Delta_\phi)^2 + 4\Delta_M^2}}{2} z\right)$$

$$= \frac{4\omega^2 B^2 \sin^2\left(\frac{\sqrt{M^2(m_\phi^2 - \omega_p^2)^2 + 4\omega^2 B^2}}{4\omega M} z\right)}{M^2(m_\phi^2 - \omega_p^2)^2 + 4\omega^2 B^2} \tag{64}$$

In the weak mixing limit we have that $\theta \ll 1$ and therefore $\frac{1}{2}\tan^{-1}\left(\frac{2\Delta_M}{\Delta_\gamma - \Delta_\phi}\right) \ll 1$ which implies that $\frac{\Delta_M}{\Delta_\gamma - \Delta_\phi} \ll 1$, and thus $\Delta_\gamma - \Delta_\phi \gg \Delta_M$. Therefore the probability becomes;

$$P_{\gamma\leftrightarrow\phi} = \frac{4\Delta_M^2}{(\Delta_\gamma - \Delta_\phi)^2} \sin^2\left(\frac{(\Delta_\gamma - \Delta_\phi) z}{2}\right) \tag{65}$$

now since $2\theta = \tan^{-1}\left(\frac{2\Delta_M}{\Delta_\gamma - \Delta_\phi}\right) \approx \frac{2\Delta_M}{\Delta_\gamma - \Delta_\phi}$ we obtain;

$$P_{\gamma\leftrightarrow\phi} \approx 4\theta^2 \sin^2\left(\frac{\Delta_{osc} z}{2}\right) \tag{66}$$

where $\Delta_{osc} = \Delta_\gamma - \Delta_\phi$ is the momentum difference between relativistic chameleons of energy ω and photons of the same energy. In the strong coupling regime we have that $|\Delta_\gamma - \Delta_\phi| \ll \Delta_M$ such that

$$P_{\gamma\leftrightarrow\phi} \approx \sin^2(\Delta_M z) \tag{67}$$

which is the same as the one obtained by Raffelt and Stodolsky [20]. Now if we relax the condition made in equation(48) the system in equation(47) can be solved by diagonalising the matrix below

$$A = \begin{pmatrix} \Delta_\gamma & \Delta_M \\ \Delta_M & \Delta_\phi \end{pmatrix} \tag{68}$$

with $\Delta_\gamma = -\omega_p^2$, $\Delta_M = \frac{B\omega}{M}$ and $\Delta_\phi = -m_\phi^2$. Therefore A can be diagonalised by a rotation matrix

$$P = \begin{pmatrix} \cos\theta & \sin\theta \\ -\sin\theta & \cos\theta \end{pmatrix}, \tag{69}$$

such that $A = PDP^{-1}$, with

$$D = \begin{pmatrix} \lambda_+ & 0 \\ 0 & \lambda_- \end{pmatrix}, \tag{70}$$

where $\lambda_\pm$ are the eigenvalues of the matrix A given by

$$\lambda_\pm = -\frac{(\omega_p^2 + m_\phi^2)}{2} \pm \frac{\sqrt{(\omega_p^2 - m_\phi^2)^2 + 4B^2\omega^2/M^2}}{2} \tag{71}$$

$$= \Lambda \pm \Omega \tag{72}$$

Now we define

$$k_\pm = \sqrt{\omega^2 + \lambda_\pm} \tag{73}$$

Again if we consider a beam with frequency ω in the primed(interacting) fields travelling in the $z-$direction of the following form

$$\begin{bmatrix} \vec{\Psi}'_{\gamma}(z,t) \\ \Psi'_{\phi}(z,t) \end{bmatrix} = \begin{pmatrix} e^{i(\omega t - k_+ z)} & 0 \\ 0 & e^{i(\omega t - k_- z)} \end{pmatrix} \begin{bmatrix} \vec{\Psi}'_{\gamma}(0,t) \\ \Psi'_{\phi}(0,t) \end{bmatrix} \tag{74}$$

We let the transfer matrix $\mathcal{T}(z,t)$ be calculated as follows

$$\mathcal{T}(z,t) = \begin{pmatrix} \cos\theta & -\sin\theta \\ \sin\theta & \cos\theta \end{pmatrix} \begin{pmatrix} e^{i(\omega t - k_+ z)} & 0 \\ 0 & e^{i(\omega t - k_- z)} \end{pmatrix} \begin{pmatrix} \cos\theta & \sin\theta \\ -\sin\theta & \cos\theta \end{pmatrix}$$

$$= e^{i\omega t} \begin{pmatrix} [e^{-ik_+ z}\cos^2\theta + e^{-ik_- z}\sin^2\theta] & \frac{1}{2}\sin 2\theta[e^{-ik_+ z} - e^{-ik_- z}] \\ \frac{1}{2}\sin 2\theta[e^{-ik_+ z} - e^{-ik_- z}] & [e^{-ik_+ z}\sin^2\theta + e^{-ik_- z}\cos^2\theta] \end{pmatrix} \tag{75}$$

if $k_+^2 < 0$ and $k_-^2 < 0$, this is case where both the chameleon and the photon cannot propagate through the medium then the probability is given by

$$P_{\gamma\leftrightarrow\phi} = \frac{1}{4}\sin^2 2\theta \left|e^{-zk_+} - e^{-zk_-}\right|^2 \approx 0 \tag{76}$$

Since $zk_\pm \approx 0$. While when $k_+^2 < 0$ and $k_-^2 > 0$, the photon cannot propagate while the chameleon can propagate through the medium, thus we get that the probability is

$$\begin{aligned} P_{\gamma\leftrightarrow\phi} &= \frac{1}{4}\sin^2 2\theta \left|e^{-zk_+} - e^{-izk_-}\right|^2 \\ &\approx \frac{1}{2}\sin^2 2\theta \left[1 - \cos\left([k_-]\, z\right)\right] \end{aligned} \tag{77}$$

Since $e^{-zk_+} \approx 1$. In the case where $k_+^2 > 0$ and $k_-^2 < 0$ the chameleon cannot propagate while the photon can propagate through the medium then the probability is simply

$$\begin{aligned} P_{\gamma\leftrightarrow\phi} &= \frac{1}{4}\sin^2 2\theta \left|e^{-izk_+} - e^{-zk_-}\right|^2 \\ &\approx \frac{1}{2}\sin^2 2\theta \left[1 - \cos\left([k_+]\, z\right)\right] \end{aligned} \tag{78}$$

here we also have that $e^{-zk_-} \approx 1$. If $k_+^2 > 0$ and $k_-^2 > 0$, then both the photon and the chameleon can propagate through the medium, thus the chameleon-photon oscillation probability becomes

$$P_{\gamma\leftrightarrow\phi} = \frac{1}{2}\sin^2 2\theta\,[1-\cos\left([\Delta k]\,z\right)] \tag{79}$$

where $\Delta k = k_- - k_+$, and when substituting back for $\sin^2 2\theta$ we obtain the probability as follows;

$$P_{\gamma\leftrightarrow\phi} = \frac{4B^2\omega^2\sin^2\left([\Delta k]\,z/2\right)}{M^2(m_\phi^2-\omega_p^2)^2+4B^2\omega^2}. \tag{80}$$

3.2 Chameleon and Photon Evolution Equations

From equation(75) we can see that the evolution equations for the chameleon and the photon fields are as follows, the photon is given by

$$\vec{\Psi}_{\gamma\|}(z) = \left|\vec{\Psi}_{\gamma\|}(0)\right|\left[e^{-ik_+z}\cos^2\theta + e^{-ik_-z}\sin^2\theta\right] + |\Psi_\phi(0)|\,\frac{1}{2}\sin 2\theta\left[e^{-ik_+z}-e^{-ik_-z}\right] \tag{81}$$

and the Chameleon-ϕ field is given by the following

$$\Psi_\phi(z) = |\Psi_\phi(0)|\left[e^{-ik_+z}\sin^2\theta + e^{-ik_-z}\cos^2\theta\right] + \left|\vec{\Psi}_{\gamma\|}(0)\right|\frac{1}{2}\sin 2\theta\left[e^{-ik_+z}-e^{-ik_-z}\right] \tag{82}$$

Equations (81) and (82) can be rewritten in th following way,

$$\vec{\Psi}_{\gamma\|}(z) = \left|\vec{\Psi}_{\gamma\|}(0)\right|\sqrt{1-P_{\gamma\leftrightarrow\phi}}e^{\{-i(k_-z-\delta_c)\}} + |\Psi_\phi(0)|\sqrt{P_{\gamma\leftrightarrow\phi}}e^{\{-i(k_+z-\psi)\}} \tag{83}$$

$$\Psi_\phi(z) = |\Psi_\phi(0)|\sqrt{1-P_{\gamma\leftrightarrow\phi}}e^{\{-i(k_-z-\delta_s)\}} + \left|\vec{\Psi}_{\gamma\|}(0)\right|\sqrt{P_{\gamma\leftrightarrow\phi}}e^{\{-i(k_+z-\psi)\}} \tag{84}$$

where the phase differences are given by δ_c, δ_s and ψ as follows.

$$\delta_c = \sin^{-1}\left(\frac{\cos^2\theta\sin(\Delta kz)}{\sqrt{1-P_{\gamma\leftrightarrow\phi}}}\right) \tag{85}$$

$$\delta_s = \sin^{-1}\left(\frac{\sin^2\theta\sin(\Delta kz)}{\sqrt{1-P_{\gamma\leftrightarrow\phi}}}\right) \tag{86}$$

$$\psi = \sin^{-1}\left(\cos(\Delta kz/2)\right) \tag{87}$$

$$\tag{88}$$

And the oscillation probability is

$$P_{\gamma\leftrightarrow\phi} = \sin^2 2\theta \sin^2\left([\Delta k]\, z/2\right) \tag{89}$$

Furthermore we can express equations (83) and (84) in this way

$$\vec{\Psi}_{\gamma\parallel}(z) = \left|\vec{\Psi}_{\gamma\parallel}(z)\right| \exp\left[-i\left(k_- z - \delta_c - \sin^{-1}\left(\frac{|\Psi_\phi(0)|\sqrt{P_{\gamma\leftrightarrow\phi}}\sin(\Delta kz+\psi-\delta_c)}{\left|\vec{\Psi}_{\gamma\parallel}(z)\right|}\right)\right)\right] \tag{90}$$

$$\Psi_\phi(z) = |\Psi_\phi(z)| \exp\left[-i\left(k_- z - \delta_s - \sin^{-1}\left(\frac{\left|\vec{\Psi}_{\gamma\parallel}(0)\right|\sqrt{P_{\gamma\leftrightarrow\phi}}\sin(\Delta kz+\psi-\delta_s)}{|\Psi_\phi(z)|}\right)\right)\right] \tag{91}$$

where the chameleon-ϕ and photon amplitudes as function of distance are

$$\begin{aligned}\left|\vec{\Psi}_{\gamma\parallel}(z)\right|^2 = {} & \left|\vec{\Psi}_{\gamma\parallel}(0)\right|^2 (1-P_{\gamma\leftrightarrow\phi}) + |\Psi_\phi(0)|^2 P_{\gamma\leftrightarrow\phi} \\ & + 2\,|\Psi_\phi(0)|\left|\vec{\Psi}_{\gamma\parallel}(0)\right|\sqrt{P_{\gamma\leftrightarrow\phi}(1-P_{\gamma\leftrightarrow\phi})}\cos(\Delta kz+\psi-\delta_c)\end{aligned} \tag{92}$$

$$\begin{aligned}|\Psi_\phi(z)|^2 = {} & |\Psi_\phi(0)|^2 (1-P_{\gamma\leftrightarrow\phi}) + \left|\vec{\Psi}_{\gamma\parallel}(0)\right|^2 P_{\gamma\leftrightarrow\phi} \\ & + 2\,|\Psi_\phi(0)|\left|\vec{\Psi}_{\gamma\parallel}(0)\right|\sqrt{P_{\gamma\leftrightarrow\phi}(1-P_{\gamma\leftrightarrow\phi})}\cos(\Delta kz+\psi-\delta_s)\end{aligned} \tag{93}$$

3.3 Stokes parameters

Following the work by Burrage[21], we define the stokes parameters for the chameleon-photon system as follows.

$$I_\gamma = \left|\vec{\Psi}_{\gamma\|}(z,t)\right|^2 + \left|\vec{\Psi}_{\gamma\perp}(z,t)\right|^2 \tag{94}$$

$$Q = \left|\vec{\Psi}_{\gamma\|}(z,t)\right|^2 - \left|\vec{\Psi}_{\gamma\perp}(z,t)\right|^2 \tag{95}$$

$$U + iV = 2\left|\vec{\Psi}^*_{\gamma\|}(z,t)\vec{\Psi}_{\gamma\perp}(z,t)\right| \tag{96}$$

$$J + iK = 2\left|\vec{\Psi}^*_{\gamma\perp}(z,t)\Psi_\phi(z,t)\right| \tag{97}$$

$$L + iM = 2\left|\vec{\Psi}^*_{\gamma\|}(z,t)\Psi_\phi(z,t)\right| \tag{98}$$

Where I_γ is the total photon flux. The amount of linear polarization is described by Q, U, J and L whereas the amount of circular polarization is given by V, K and M. The flux of the photon field polarized perpendicular to the external magnetic field evolves as follows;

$$\left|\vec{\Psi}_{\gamma\perp}(z,t)\right|^2 = \left|\vec{\Psi}^*_{\gamma\perp}(z,t)\right|^2 = \left|\vec{\Psi}_{\gamma\perp}(0,t)\right|^2 \tag{99}$$

since the chameleon does not mix with the polarization ot the magnetic field that is perpendicular to the external magnetic field, it only mixes with the photon polarization which is parallel to the external magnetic field. The photon state that mixes with the chameleon after travelling through a single magnetic domain is give by the first component of equation (74) as follows;

$$\vec{\Psi}_{\gamma\|}(z,t) = \left[e^{-ik_+ z}\cos^2\theta + e^{-ik_- z}\sin^2\theta\right]\vec{\Psi}_{\gamma\|}(0,t) + \frac{1}{2}\sin 2\theta[e^{-ik_+ z} - e^{-ik_- z}]\Psi_\phi(0,t) \tag{100}$$

Then the flux is given by the following;

$$\left|\vec{\Psi}_{\gamma\|}(z,t)\right|^2 = \vec{\Psi}^*_{\gamma\|}(z,t)\vec{\Psi}_{\gamma\|}(z,t) \tag{101}$$

$$\begin{aligned}
&= \left|\vec{\Psi}_{\gamma\|}(0,t)\right|^2 \left(\cos^4\theta + \sin^4\theta + \sin^2\theta\cos^2\theta\left[e^{-i(\Delta k)z} + e^{i(\Delta k)z}\right]\right) \\
&\quad + \frac{1}{4}\left|\Psi_\phi(0,t)\right|^2 \sin^2 2\theta \left(2 - \left[e^{-i(\Delta k)z} + e^{i(\Delta k)z}\right]\right) \\
&\quad + \frac{1}{2}\left|\vec{\Psi}_{\gamma\|}(0,t)\right| \left|\Psi^*_\phi(0,t)\right| \sin 2\theta \left(\cos 2\theta + e^{-i(\Delta k)z}\sin^2\theta - e^{i(\Delta k)z}\cos^2\theta\right) \\
&\quad + \frac{1}{2}\left|\vec{\Psi}^*_{\gamma\|}(0,t)\right| \left|\Psi_\phi(0,t)\right| \sin 2\theta \left(\cos 2\theta + e^{i(\Delta k)z}\sin^2\theta - e^{-i(\Delta k)z}\cos^2\theta\right)
\end{aligned} \tag{102}$$

$$\begin{aligned}
&= \left|\vec{\Psi}_{\gamma\|}(0,t)\right|^2 \left(1 - \sin^2 2\theta \sin^2([\Delta k]\frac{z}{2})\right) + \left|\Psi_\phi(0,t)\right|^2 \sin^2 2\theta \sin^2([\Delta k]\frac{z}{2}) \\
&\quad + 2\left|\vec{\Psi}_{\gamma\|}(0,t)\right| \left|\Psi_\phi(0,t)\right| \sin 2\theta \cos 2\theta \sin^2([\Delta k]\frac{z}{2})
\end{aligned} \tag{103}$$

$$\begin{aligned}
&= P_{\gamma\leftrightarrow\phi}(z)\left[\left|\Psi_\phi(0,t)\right|^2 - \left|\vec{\Psi}_{\gamma\|}(0,t)\right|^2 + 2\left|\vec{\Psi}_{\gamma\|}(0,t)\right| \left|\Psi_\phi(0,t)\right| \cot 2\theta\right] \\
&\quad + \left|\vec{\Psi}_{\gamma\|}(0,t)\right|^2
\end{aligned} \tag{104}$$

Following the same argument as above we arrive at the chameleon flux below,

$$\begin{aligned}
\left|\Psi_\phi(z,t)\right|^2 = P_{\gamma\leftrightarrow\phi}(z)&\left[\left|\vec{\Psi}_{\gamma\|}(0,t)\right|^2 - \left|\Psi_\phi(0,t)\right|^2 - 2\left|\vec{\Psi}_{\gamma\|}(0,t)\right| \left|\Psi_\phi(0,t)\right| \cot 2\theta\right] \\
&+ \left|\Psi_\phi(0,t)\right|^2
\end{aligned} \tag{105}$$

Therefore the Stokes parameters become,

$$I_\gamma(z,t) = I_\gamma(0,t) + P_{\gamma\leftrightarrow\phi}(z)\left[I_\phi(0,t) - I_{\gamma\|}(0,t) + 2\sqrt{I_{\gamma\|}(0,t)I_\phi(0,t)}\cot 2\theta\right] \tag{106}$$

$$Q = Q(0,t) + P_{\gamma\leftrightarrow\phi}(z)\left[I_\phi(0,t) - I_{\gamma\|}(0,t) + 2\sqrt{I_{\gamma\|}(0,t)I_\phi(0,t)}\cot 2\theta\right] \tag{107}$$

$$\begin{aligned}
U + iV &= 2\left|\vec{\Psi}^*_{\gamma\|}(z,t)\vec{\Psi}_{\gamma\perp}(z,t)\right| \\
&= 2\left[e^{ik_+ z}\cos^2\theta + e^{ik_- z}\sin^2\theta\right] \left|\vec{\Psi}^*_{\gamma\|}(0,t)\right| \left|\vec{\Psi}_{\gamma\perp}(0,t)\right| \\
&\quad + \sin 2\theta[e^{ik_+ z} - e^{ik_- z}] \left|\Psi^*_\phi(0,t)\right| \left|\vec{\Psi}_{\gamma\perp}(0,t)\right|
\end{aligned} \tag{108}$$

where

$$U = 2\sqrt{I_{\gamma\parallel}(0,t)I_{\gamma\perp}(0,t)}\left[\cos^2\theta\cos(k_+z) + \sin^2\theta\cos(k_-z)\right] + \sqrt{I_{\gamma\perp}(0,t)I_{\phi}(0,t)}\left[\sin 2\theta\left(\cos(k_+z) - \cos(k_-z)\right)\right] \tag{109}$$

and

$$V = 2\sqrt{I_{\gamma\parallel}(0,t)I_{\gamma\perp}(0,t)}\left[\cos^2\theta\sin(k_+z) + \sin^2\theta\sin(k_-z)\right] + \sqrt{I_{\gamma\perp}(0,t)I_{\phi}(0,t)}\left[\sin 2\theta\left(\sin(k_+z) - \sin(k_-z)\right)\right] \tag{110}$$

For the linear and circular polarization parameters due to the chameleon and photon states we have the following:

$$J + iK = 2\left|\vec{\Psi}^*_{\gamma\perp}(z,t)\Psi_{\phi}(z,t)\right|$$

$$J = 2\sqrt{I_{\gamma\parallel}(0,t)I_{\gamma\perp}(0,t)}\left[\sin 2\theta\left(\cos(k_+z) - \cos(k_-z)\right)\right] + \sqrt{I_{\gamma\perp}(0,t)I_{\phi}(0,t)}\left[\cos^2\theta\cos(k_+z) + \sin^2\theta\cos(k_-z)\right] \tag{111}$$

$$K = 2\sqrt{I_{\gamma\parallel}(0,t)I_{\gamma\perp}(0,t)}\left[\sin 2\theta\left(\sin(k_+z) - \sin(k_-z)\right)\right] - \sqrt{I_{\gamma\perp}(0,t)I_{\phi}(0,t)}\left[\cos^2\theta\sin(k_+z) + \sin^2\theta\sin(k_-z)\right] \tag{112}$$

Finally we calculate $L + iM$ to be:

$$\begin{aligned} L + iM &= 2\left|\vec{\Psi}^*_{\gamma\parallel}(z,t)\Psi_{\phi}(z,t)\right| \\ &= \left|\vec{\Psi}_{\gamma\parallel}(0,t)\right|^2\sin 2\theta\left(\cos^2\theta\left[1 - e^{-i(\Delta k)z}\right] + \sin^2\theta\left[e^{i(\Delta k)z} - 1\right]\right) \\ &\quad + 2\left|\vec{\Psi}^*_{\gamma\parallel}(0,t)\right|\left|\Psi_{\phi}(0,t)\right|\left(2\sin^2\theta\cos^2\theta + e^{-i(\Delta k)z}\cos^4\theta + e^{i(\Delta k)z}\sin^4\theta\right) \\ &\quad + \left|\vec{\Psi}_{\gamma\parallel}(0,t)\right|\left|\Psi^*_{\phi}(0,t)\right|\frac{\sin^2 2\theta}{2}\left[2 - 2\cos([\Delta k]z)\right] \\ &\quad - \left|\Psi_{\phi}(0,t)\right|^2\sin 2\theta\left(\cos^2\theta\left[1 - e^{-i(\Delta k)z}\right] + \sin^2\theta\left[e^{i(\Delta k)z} - 1\right]\right) \end{aligned} \tag{113}$$

$$= \left[\left|\vec{\Psi}_{\gamma\|}(0,t)\right|^2 - |\Psi_\phi(0,t)|^2\right] \sin 2\theta \left(\cos 2\theta \left(1 - \cos([\Delta k]z)\right) + i \sin([\Delta k]z)\right)$$
$$+ 2\left|\vec{\Psi}^*_{\gamma\|}(0,t)\right| |\Psi_\phi(0,t)| \left[\cos([\Delta k]z) + \sin^2 2\theta \left(1 - \cos([\Delta k]z)\right)\right]$$
$$- 2i\left|\vec{\Psi}^*_{\gamma\|}(0,t)\right| |\Psi_\phi(0,t)| \cos 2\theta \sin([\Delta k]z) \tag{114}$$

Therefore L and M as given by the real and the imaginary parts of $L + iM$ as follows;

$$L = \left[\left|\vec{\Psi}_{\gamma\|}(0,t)\right|^2 - |\Psi_\phi(0,t)|^2\right] \sin 2\theta \cos 2\theta \left(1 - \cos([\Delta k]z)\right)$$
$$+ 2\left|\vec{\Psi}^*_{\gamma\|}(0,t)\right| |\Psi_\phi(0,t)| \left[\cos([\Delta k]z) + \sin^2 2\theta \left(1 - \cos([\Delta k]z)\right)\right] \tag{115}$$

$$M = \sin([\Delta k]z) \left(\left[\left|\vec{\Psi}_{\gamma\|}(0,t)\right|^2 - |\Psi_\phi(0,t)|^2\right] \sin 2\theta - 2\left|\vec{\Psi}^*_{\gamma\|}(0,t)\right| |\Psi_\phi(0,t)| \cos 2\theta\right) \tag{116}$$

3.4 Mixing in inhomogeneous magnetic fields

Considering the perturbative solution of the Schrödinger type equation outlined in [20], we can rewrite equation (49) as follows;

$$i\partial_z \vec{\Psi}(z) = (\mathcal{H}_0(z) + \mathcal{H}_1(z))\vec{\Psi}(z) \tag{117}$$

where $\vec{\Psi}(z) = (\vec{\Psi}_{\gamma\|}(z), \Psi_\phi(z))$,

$$\mathcal{H}_0(z) = \begin{pmatrix} \omega - \frac{\omega_p^2(z)}{2\omega} & 0 \\ 0 & \omega - \frac{m_\phi^2(z)}{2\omega} \end{pmatrix} \tag{118}$$

and

$$\mathcal{H}_1(z) = \begin{pmatrix} 0 & \frac{B(z)}{2M} \\ \frac{B(z)}{2M} & 0 \end{pmatrix} \tag{119}$$

The uncoupled system is given by $\frac{B(z)}{2M} \to 0$, this system has a solution of the form

$$\vec{\Psi}(z) = \mathcal{U}(z)\vec{\Psi}(z_0) \tag{120}$$

where $\mathcal{U}(z) = \exp\left(-i\int_{z_0}^{z}\mathcal{H}_0(z')dz'\right)$. We define the interaction transformation by means of a unitary transformation $\vec{\Psi}_{int}(z) = \mathcal{U}^{\dagger}(z)\vec{\Psi}(z)$, then by differentiating both sides with respect to z and using the fact that $\mathcal{U}^{\dagger}(z)\mathcal{H}_0(z)\mathcal{U}(z) = \mathcal{H}_0(z)$, we obtain the following equation for the interacting fields.

$$i\partial_z\vec{\Psi}_{int}(z) = \mathcal{H}_{int}(z)\vec{\Psi}_{int}(z) \tag{121}$$

with $\mathcal{H}_{int}(z) = \mathcal{U}^{\dagger}(z)\mathcal{H}_1(z)\mathcal{U}(z)$, the solution to equation (121) can be found order buy order from the integral equation

$$\vec{\Psi}_{int}(z) = \vec{\Psi}_{int}(z_0) - i\int_{z_0}^{z}\mathcal{H}_{int}(z')\vec{\Psi}_{int}(z')dz' \tag{122}$$

the zeroth-order solution is $\vec{\Psi}^{(0)}_{int}(z) = \vec{\Psi}_{int}(z_0)$, substituting the zeroth-order solution back in equation (122) we can obtain the first-order solution to be

$$\begin{aligned}\vec{\Psi}^{(1)}_{int}(z) &= \vec{\Psi}_{int}(z_0) - i\int_{z_0}^{z}\mathcal{H}_{int}(z')dz'\vec{\Psi}_{int}(z_0)\\ &= \vec{\Psi}_{int}(z_0)\left(1 - i\int_{z_0}^{z}\mathcal{H}_{int}(z')dz'\right)\end{aligned} \tag{123}$$

by substituting equation (123) into the right hand side of equation (122) we obtain the second-order solution as

$$\vec{\Psi}^{(2)}_{int}(z) = \vec{\Psi}_{int}(z_0)\left(1 - i\int_{z_0}^{z}\mathcal{H}_{int}(z')dz' - \int_{z_0}^{z}dz'\int_{z_0}^{z'}dz''\mathcal{H}_{int}(z')\mathcal{H}_{int}(z'')\right). \tag{124}$$

The chameleon-photon oscillation probability form the first-order solution is

$$\begin{aligned}P_{\gamma\leftrightarrow\phi} &= \left|\int_{z_0}^{z}\mathcal{H}_{int}(z')dz'\right|^2\\ &= \left|\int_{z_0}^{z}\frac{B(z')}{2M}\exp\left(i\int_{z_0}^{z'}\frac{\omega_p^2(z'') - m_{\phi}^2(z'')}{2\omega}dz''\right)dz'\right|^2\end{aligned} \tag{125}$$

where

$$\mathcal{H}_{int}(z') = \begin{pmatrix} 0 & \frac{B(z')}{2M}\exp\left(-i\int_{z_0}^{z'}\frac{\omega_p^2(z'')-m_\phi^2(z'')}{2\omega}dz''\right) \\ \frac{B(z')}{2M}\exp\left(i\int_{z_0}^{z'}\frac{\omega_p^2(z'')-m_\phi^2(z'')}{2\omega}dz''\right) & 0 \end{pmatrix} \tag{126}$$

In a region of length L with a homogeneous magnetic field, we have that at any distance z in the range $0 < z > L$ the magnetic field $B(z) = \overline{B}$, the plasma frequency $\omega_p(z) = \overline{\omega}_p$ and the chameleon mass $m_\phi(z) = \overline{m}_\phi$ are constant, hence the probability in equation (125) becomes

$$\begin{aligned} P_{\gamma\leftrightarrow\phi} &= \left|\int_0^L \frac{\overline{B}}{2M}\exp\left(i\int_0^{z'}\frac{\overline{\omega}_p^2-\overline{m}_\phi^2}{2\omega}dz''\right)dz'\right|^2 \\ &= \frac{\overline{B}^2}{4M^2}\left|\int_0^L \exp\left[i\left(\frac{\overline{\omega}_p^2-\overline{m}_\phi^2}{2\omega}\right)z'\right]dz'\right|^2 \qquad (127) \\ &= \frac{\overline{B}^2\omega^2}{M^2(\overline{\omega}_p^2-\overline{m}_\phi^2)^2}\left|\exp\left[i\left(\frac{\overline{\omega}_p^2-\overline{m}_\phi^2}{2\omega}\right)L\right]-1\right|^2 \\ &= \frac{\overline{B}^2\omega^2}{M^2(\overline{\omega}_p^2-\overline{m}_\phi^2)^2}\left(2-2\cos\left[\left(\frac{\overline{\omega}_p^2-\overline{m}_\phi^2}{2\omega}\right)L\right]\right) \\ &= \frac{4\overline{B}^2\omega^2}{M^2(\overline{\omega}_p^2-\overline{m}_\phi^2)^2}\sin^2\left[\left(\frac{\overline{\omega}_p^2-\overline{m}_\phi^2}{4\omega}\right)L\right] \qquad (128) \end{aligned}$$

which is similar to the weak mixing case where $\left|\frac{\overline{\omega}_p^2-\overline{m}_\phi^2}{\omega}\right| \gg \frac{B}{M}$ given by equation (65) obtained previously. From equation (128) we can show that when $\left|\frac{\overline{\omega}_p^2-\overline{m}_\phi^2}{\omega}\right| \ll \frac{B}{M} < 1$ for all values of the chameleon-photon coupling constant used in this discussion, equation (128) can be written as

$$\begin{aligned} P_{\gamma\leftrightarrow\phi} &\approx \frac{4\overline{B}^2\omega^2}{M^2(\overline{\omega}_p^2-\overline{m}_\phi^2)^2}\left[\left(\frac{\overline{\omega}_p^2-\overline{m}_\phi^2}{4\omega}\right)L\right]^2 \\ &\approx \frac{1}{4}\frac{\overline{B}^2}{M^2}L^2 \qquad (129) \end{aligned}$$

equation (129) is similar to equation (67) for values of $\Delta_M z \ll 1$.

3.5 Mixing in randomly oriented magnetic fields

Following the derivation outlined in [22], we want to find the chameleon and photon fluxes after passing through N magnetic domains of equal length with homogeneous magnetic field in each domain. The initial state is

$$\alpha_{\parallel}(0)|\vec{\Psi}_{\gamma\parallel}\rangle + \alpha_{\perp}(0)|\vec{\Psi}_{\gamma\perp}\rangle + \alpha_{\phi}(0)|\Psi_{\phi}\rangle \tag{130}$$

where $|\vec{\Psi}_{\gamma\parallel}\rangle$ and $|\vec{\Psi}_{\gamma\perp}\rangle$ are the photon states parallel and perpendicular to the magnetic field in the first domain and $|\Psi_{\phi}\rangle$ is the chameleon. In terms of fluxes we have that

$$I_{\gamma}(0) \sim |\alpha_{\parallel}(0)|^2 + |\alpha_{\perp}(0)|^2 \tag{131}$$

$$I_{\phi}(0) \sim |\alpha_{\phi}(0)|^2. \tag{132}$$

where $\alpha_{\parallel}(0)$, $\alpha_{\perp}(0)$ and $\alpha_{\phi}(0)$ are the photon($\parallel, \perp$) and chameleon amplitudes. In the n^{th} domain the magnetic field is tilted by an angle ϑ_n compared to the first domain, therefore the two photon states become

$$|\vec{\Psi}^n_{\gamma\parallel}\rangle = \cos\vartheta_n|\vec{\Psi}_{\gamma\parallel}\rangle + \sin\vartheta_n|\vec{\Psi}_{\gamma\perp}\rangle \tag{133}$$

$$|\vec{\Psi}^n_{\gamma\perp}\rangle = -\sin\vartheta_n|\vec{\Psi}_{\gamma\parallel}\rangle + \cos\vartheta_n|\vec{\Psi}_{\gamma\perp}\rangle \tag{134}$$

where ϑ_n is a random variable, therefore the average of $\cos^2\vartheta_n \sim \sin^2\vartheta_n \sim \frac{1}{2}$. Which implies that equation(131) becomes $I^n_{\gamma} \sim 2I^n_{\gamma\perp} \sim 2I^n_{\gamma\parallel}$. Let the conversion probability for incident photons in a single magnetic domain be given by $P_{\gamma\leftrightarrow\phi} = P$. Therefore we can write down the fluxes in the n^{th} domain as follows

$$I_{\gamma\perp}(y) = I_{\gamma\perp}(0) = \frac{I_{\gamma}(0)}{2} \tag{135}$$

$$I_{\gamma\parallel}(y) = I_{\gamma\parallel}(0)[1-P] + I_{\phi}(0)P = \frac{I_{\gamma}(0)}{2}[1-P] + I_{\phi}(0)P \tag{136}$$

in which

$$I_\gamma(y) = I_{\gamma\perp}(y) + I_{\gamma\parallel}(y) = \frac{I_\gamma(0)}{2}[2-P] + I_\phi(0)P \tag{137}$$

and

$$I_\phi(y) = I_\phi(0)[1-P] + I_{\gamma\parallel}(0)P = I_\phi(0)[1-P] + \frac{I_\gamma(0)}{2}P. \tag{138}$$

Now we subtract twice equation (138) from equation (137) to get

$$I_\gamma(y) - 2I_\phi(y) = [I_\gamma(0) - 2I_\phi(0)] + P[3I_\phi(0) - \frac{3}{2}I_\gamma(0)] \tag{139}$$

$$I_\gamma(y) - 2I_\phi(y) = \left[1 - \frac{3P}{2}\right]^N [I_\gamma(0) - 2I_\phi(0)] \tag{140}$$

by letting $y = NL_d$, where L_d and N are the domain length and number of magnetic domains respectively, therefore by substituting equation (138) into (140) and adding $3 \times I_\gamma(y)$ to the new equation one arrives at the photon flux in the n^{th} domain given in terms of initial photon and chameleon fluxes as follows

$$I_\gamma(y) = \frac{2}{3}[I_\gamma(0) + I_\phi(0)] + \frac{1}{3}\left[1 - \frac{3P}{2}\right]^N [I_\gamma(0) - 2I_\phi(0)] \tag{141}$$

and

$$I_\phi(y) = \frac{1}{3}[I_\gamma(0) + I_\phi(0)] - \frac{1}{3}\left[1 - \frac{3P}{2}\right]^N [I_\gamma(0) - 2I_\phi(0)] \tag{142}$$

. An alternative derivation is obtained by noting that from equations (137) and (138) one gets the following system when photons transverse a single magnetic domain,

$$\begin{bmatrix} I_\gamma(y) \\ \\ I_\phi(y) \end{bmatrix} = \begin{pmatrix} 1 - \frac{P}{2} & P \\ \\ \frac{P}{2} & 1 - P \end{pmatrix} \begin{bmatrix} I_\gamma(0) \\ \\ I_\phi(0) \end{bmatrix} = S \begin{bmatrix} I_\gamma(0) \\ \\ I_\phi(0) \end{bmatrix} \tag{143}$$

with matrix S being a stochastic or Markov matrix since P is the probability and the sum of the values in each column is 1. This matrix is diagonalizable, in fact there exist a matrix Q such that $\mathcal{D} = Q^{-1}SQ$, in which

$$Q = \begin{pmatrix} 2 & -1 \\ \\ 1 & 1 \end{pmatrix} \tag{144}$$

and

$$\mathcal{D} = \begin{pmatrix} 1 & 0 \\ 0 & \left(1 - \frac{3P}{2}\right) \end{pmatrix} \tag{145}$$

hence $S = Q\mathcal{D}Q^{-1}$, then in the n^{th} domain it is well known that $S^N = Q\mathcal{D}^N Q^{-1}$ see proof below

Proof. Let $S = Q\mathcal{D}Q^{-1}$ where Q is a invertible and $\mathcal{D}$ is diagonal matrix. Thus

$$S^2 = \left(Q\mathcal{D}Q^{-1}\right)\left(Q\mathcal{D}Q^{-1}\right)$$

$$= Q\mathcal{D}\mathcal{D}Q^{-1}$$

$$\therefore S^2 = Q\mathcal{D}^2Q^{-1}$$

and

$$S^3 = S^2\left(Q\mathcal{D}Q^{-1}\right)$$

$$= \left(Q\mathcal{D}^2Q^{-1}\right)\left(Q\mathcal{D}Q^{-1}\right)$$

$$\therefore S^3 = Q\mathcal{D}^3Q^{-1}$$

therefore by induction we have that;

$$S^N = S^{N-1}\left(Q\mathcal{D}Q^{-1}\right)$$

$$= \left(Q\mathcal{D}^{N-1}Q^{-1}\right)\left(Q\mathcal{D}Q^{-1}\right)$$

$$\therefore S^N = Q\mathcal{D}^NQ^{-1}$$

□

Therefore

$$S^N = \begin{pmatrix} 2 & -1 \\ 1 & 1 \end{pmatrix} \begin{pmatrix} 1 & 0 \\ 0 & \left(1-\frac{3P}{2}\right)^N \end{pmatrix} \begin{pmatrix} \frac{1}{3} & \frac{1}{3} \\ -\frac{1}{3} & \frac{2}{3} \end{pmatrix} \tag{146}$$

$$= \frac{1}{3} \begin{pmatrix} 2+\left(1-\frac{3P}{2}\right)^N & 2-2\left(1-\frac{3P}{2}\right)^N \\ 1-\left(1-\frac{3P}{2}\right)^N & 1+2\left(1-\frac{3P}{2}\right)^N \end{pmatrix} \tag{147}$$

which result in the following chameleon-photon system in terms of fluxes.

$$\begin{bmatrix} I_\gamma(y) \\ I_\phi(y) \end{bmatrix} = \frac{1}{3} \begin{pmatrix} 2+\left(1-\frac{3P}{2}\right)^N & 2-2\left(1-\frac{3P}{2}\right)^N \\ 1-\left(1-\frac{3P}{2}\right)^N & 1+2\left(1-\frac{3P}{2}\right)^N \end{pmatrix} \begin{bmatrix} I_\gamma(0) \\ I_\phi(0) \end{bmatrix} \tag{148}$$

Let $Q_o(y) = \left(1-\frac{3P_o}{2}\right)^{N_o}$ for the conversion from the edge of the pulsar magnetosphere [22] to the observer. In the same way let $Q_i(y) = \left(1-\frac{3P_i}{2}\right)^{N_i}$ for conversion within the pulsar magnetosphere which is from the surface of the pulsar to the edge of the pulsar magnetosphere, thus we have that

$$\begin{bmatrix} I_\gamma(y) \\ I_\phi(y) \end{bmatrix}_i = \frac{1}{3} \begin{pmatrix} 2+Q_i(y) & 2-2Q_i(y) \\ 1-Q_i(y) & 1+2Q_i(y) \end{pmatrix} \begin{bmatrix} I_\gamma(0) \\ I_\phi(0) \end{bmatrix}_i \tag{149}$$

and

$$\begin{bmatrix} I_\gamma(y) \\ I_\phi(y) \end{bmatrix}_o = \frac{1}{3} \begin{pmatrix} 2+Q_o(y) & 2-2Q_o(y) \\ 1-Q_o(y) & 1+2Q_o(y) \end{pmatrix} \begin{bmatrix} I_\gamma(y) \\ I_\phi(y) \end{bmatrix}_i \tag{150}$$

$$= \frac{1}{3} \begin{pmatrix} 2+Q_o(y)Q_i(y) & 2-2Q_o(y)Q_i(y) \\ 1-Q_o(y)Q_i(y) & 1+2Q_o(y)Q_i(y) \end{pmatrix} \begin{bmatrix} I_\gamma(0) \\ I_\phi(0) \end{bmatrix}_i \tag{151}$$

Therefore

$$P_{\gamma\leftrightarrow\gamma} = \frac{I_\gamma(y)_o}{I_\gamma(0)_i} \tag{152}$$

$$= \frac{2}{2+Q_i(y)} + Q_o(y)\frac{Q_i(y)}{2+Q_i(y)}. \tag{153}$$

4 Searching for Chameleons in Pulsar Magnetosphere

The probability of chameleon-photon conversion $P_{\gamma\leftrightarrow\phi}$ is given by equation (64). Pulsars are a good place to test for chameleon-photon mixing in astrophysics[27] because they have very strong magnetic fields(B) and emit light in a wide range of frequencies from the radio to γ-rays. But the majority of neutron stars are seen in the radio, with a small number of these sources emitting soft γ-rays and are called soft γ-ray repeaters(SGRs) or anomalous X-ray pulsars(AXPs)[28]. The rest of the pulsars are grouped in what is called "radio-quiet neutron stars"(RQNS). These objects completely lack radio emission and are usually associated with young supernova remnants(SNRs)[28].

A pulsar PSR J0437-4715 was observed with the 64m radio telescope at Parkes [29], the observations were made at frequencies 436MHz, 660MHz, 1400MHz and 1660MHz. The period (P), period derivative ($\dot{P}$), surface magnetic field (B_s) and distance to this pulsar are 5.75ms, 5.73×10^{-20}s.s^{-1} and 159.9pc respectively. For a rotating neutron star such as PSR J0437-4715, we note that for $\dot{P} > 0$ (increasing pulsar period) the time derivative of the rotational energy (E_{rot}) is negative ($\dot{E}_{rot} < 0$), where the dot on top indicate the time derivative. The rotational energy is related to the moment of inertia (I) in the following way;

$$E_{rot} = \frac{1}{2} I\Omega^2 = \frac{2\pi^2 I}{P^2}, \tag{154}$$

where Ω is the rotational angular velocity. Hence, we have that

$$\dot{E}_{rot} = \frac{-4\pi^2 I\dot{P}}{P^3}. \tag{155}$$

This energy is carried away from the neutron star through magnetic dipole radiation,

which is possible because neutron stars have very high magnetic fields, and these are a result of flux conservation during stellar collapse. If we let the perpendicular component of the magnetic moment of the neutron star be $\vec{m}_\perp$, then the magnetic energy loss is given by;

$$\dot{E}_{mag} = -\frac{2}{3c^3}\left(\frac{d^2\vec{m}_\perp}{dt^2}\right)^2, \tag{156}$$

this equation corresponds to the Poynting flux of an electric dipole radiation. If the inclined magnetic dipole of the neutron star rotates with angular velocity Ω, thus we let $\vec{m}_\perp = \vec{m}_{\perp 0}e^{-i\Omega t}$, which gives $\ddot{\vec{m}}_\perp = -\Omega^2\vec{m}_\perp$, then

$$\ddot{\vec{m}}_\perp = \frac{-4\pi^2}{P^2}\vec{m}_\perp. \tag{157}$$

Letting the perpendicular component of the magnetic moment at the surface of the neutron star be $\vec{m}_{\perp s} = B_s R^3 \sin\alpha$, where B_s is the surface magnetic field strength of the pulsar, R is the radius of the star and α is the angle of inclination of the magnetic moment to the rotational axis. Then the magnetic energy loss becomes

$$\dot{E}_{mag} = -\frac{2}{3c^3}\left(\frac{4\pi^2 B_s R^3 \sin\alpha}{P^2}\right)^2. \tag{158}$$

If we require that the loss of rotational energy be due to magnetic dipole radiation, then we obtain a condition for the surface magnetic field strength $B_s \sin\alpha$ as follows

$$B_s \sin\alpha = \left(\frac{3Ic^3\dot{P}P}{8\pi^2 R^6}\right)^{\frac{1}{2}}. \tag{159}$$

Now, since $|\sin\alpha| \leq 1$, this gives a lower bound of

$$B_s \geq \left(\frac{3Ic^3\dot{P}P}{8\pi^2 R^6}\right)^{\frac{1}{2}} \tag{160}$$

where c is the speed of light. It is well known that for a canonical pulsar with mass $M \approx 1.4M_\odot$ and a radius of $R = 10$km then the moment of inertia is $I = 2/5(MR^2) =$

10^{45}gcm^2, hence the magnetic field has a lower limit $B_s \geq 3.2 \times 10^{19} \left(\frac{P\dot{P}}{s}\right)^{1/2}$G, the above discussion can be found in [30]. The equation for the B field(far from surface) in terms of radius r and angle Θ measured from the magnetic pole can be written as

$$B(r, \Theta) = B_s \sin\alpha \left(\frac{R}{r}\right)^3 [2\cos(\Theta)\hat{r} + \sin(\Theta)\hat{\Theta}]\text{G}. \tag{161}$$

This model works quite well, but it turns out that it is difficult to deduce the inclination angle α from observations only. For instance in our case this was obtained through computer simulations to be $\approx 35^\circ$ by [31], one might also wonder if is there another mechanism that can lead to a pulsar losing rotational energy perhaps through gravitational radiation due to pulsar glitches?, but this is beyond the scope of this work. We can approximate the electron number density in the pulsar magnetosphere (outside the pulsar) given in [20] by the following equation

$$N_e = 7 \times 10^{-2}\text{cm}^{-3} \left(\frac{B_z}{Gauss}\right) \left(\frac{sec}{P}\right). \tag{162}$$

From this we can get the plasma frequency as follows

$$\omega_p = \sqrt{\frac{4\pi\alpha N_e}{m_e}}, \tag{163}$$

in which m_e is the mass of the electron and α is the fine structure constant. Radio emission altitude (R_e) in pulsar magnetosphere is found to be in the following range of R_e between

$$R_{e,min} = 32 \times 10^4 \left(\frac{f}{10^9}\right)^{-0.35} \left(\frac{\dot{P}}{10^{-15}}\right)^{0.04} \left(\frac{P}{s}\right)^{0.25} \text{m} \tag{164}$$

and

$$R_{e,max} = 48 \times 10^4 \left(\frac{f}{10^9}\right)^{-0.17} \left(\frac{\dot{P}}{10^{-15}}\right)^{0.1} \left(\frac{P}{s}\right)^{0.35} \text{m}, \tag{165}$$

where R_e is measured from the center of the neutron star, f is the photon frequency and P is the period of rotation [32, 33]. Using the non-linear theory of the spark-associated soliton model of pulsar radio emission investigated by [34, 35], we have that the total spectral power of the curvature radiation(radiation emitted by electrons in the polar cap of pulsars which are magnetically accelerated to very high energies along the open but curved field lines, this acceleration is due to curvature) is given by;

$$I_\omega \sim \frac{Q^2}{\mathcal{R}} F\left(\frac{\omega}{\omega_c}\right)\left[1-\cos\left(a\frac{\omega}{\omega_c}\right)\right]^2 \tag{166}$$

where the fraction that is emitted with a polarization perpendicular to the direction of the magnetic field, that is the component of the radiation that mixes with the chameleon scalar field is given by;

$$I_{\perp,\omega} \sim \frac{Q^2}{2\mathcal{R}}\left[F\left(\frac{\omega}{\omega_c}\right)+G\left(\frac{\omega}{\omega_c}\right)\right]\left[1-\cos\left(a\frac{\omega}{\omega_c}\right)\right]^2. \tag{167}$$

Where the component parallel to the direction of the magnetic field is give by;

$$I_{\parallel,\omega} \sim \frac{Q^2}{2\mathcal{R}}\left[F\left(\frac{\omega}{\omega_c}\right)-G\left(\frac{\omega}{\omega_c}\right)\right]\left[1-\cos\left(a\frac{\omega}{\omega_c}\right)\right]^2, \tag{168}$$

ω is the photon frequency, ω_c is the critical frequency given by;

$$\omega_c = \frac{3}{2}\frac{c}{\mathcal{R}}\gamma_b^3 \tag{169}$$

and the functions F and G can be written in terms the modified Bessel functions of the second kind as follows

$$F(\xi) = \xi\int_\xi^\infty K_{5/3}(\xi)d\xi \tag{170}$$

and

$$G(\xi) = \xi K_{2/3}(\xi) \tag{171}$$

with $\xi = \frac{\omega}{\omega_c}$. Q is the net charge of the soliton, $\mathcal{R}$ is the radius of curvature,

$$a = \frac{3}{2}\frac{\Delta}{\mathcal{R}}\gamma_b^3, \tag{172}$$

γ_b is the Lorentz factor for a beam of plasma particles and Δ is the characteristic longitudinal dimension of the soliton. The net charge of the soliton is

$$Q = eNh^2\lambda \tag{173}$$

where N is the number charge density of the bunch of particles(electrons), h is the height of the spark and $\lambda < 100$cm is the wavelength of the emitted coherent radiation.

The model described above uses curvature radiation as its primary emission mechanism, curvature radiation is the widely used mechanism because electrons move along curved field lines in the magnetospheres of pulsars. However, there are a large number of alternative theories for pulsar radio emission including maser effects and synchrotron radiation etc. Selecting between these models is still an ongoing research, but one must choose a model that has fewer parameters to fine tune and gives roughly similar predictions with all the other viable models, such that if you change a model, that does not impact to much on your conclusions, of which this is the criteria followed here.

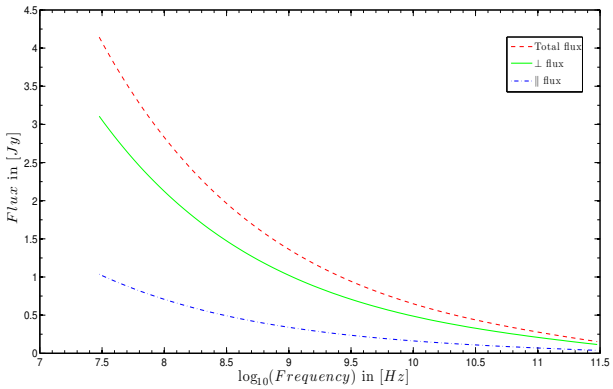

Figure 7: The plot of the flux emitted by a pulsar versus the log of frequency.

5 Results

5.1 Constraining β_γ using pulsar spectrum

5.1.1 Flux reduction

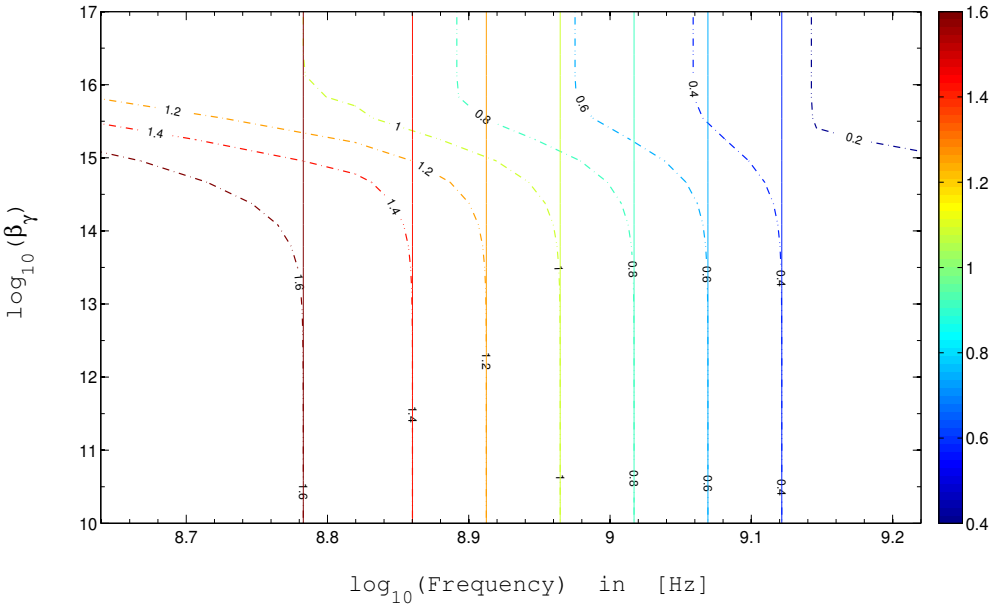

Figure 8: Here is a contour plot of the flux from the pulsar (PSR J0437-4715) as a function of $\log_{10}(\beta_\gamma)$ the photon-chameleon coupling constant (vertical axis) and the observed frequency (horizontal axis), the vertical solid lines show the flux before photon-chameleon mixing (emission) and the dashed-dotted lines shows the flux after photon-chameleon mixing (detection). The flux units (of the contours) used in this plot are the Jansky [Jy].

From figure(8) one can see that the observed flux (dotted lines) starts to deviate significantly from the initial/emitted flux (solid lines) due to chameleon-photon mixing in the region where $\beta_\gamma > 10^{13}$ at all the observed frequencies. Figure (9) below shows the χ^2

statistic for comparing the data to the predicted spectra at different coupling constant values, with the minimum reached in the range $\beta_\gamma > 10^6$, thus our calculation will be done in this region.

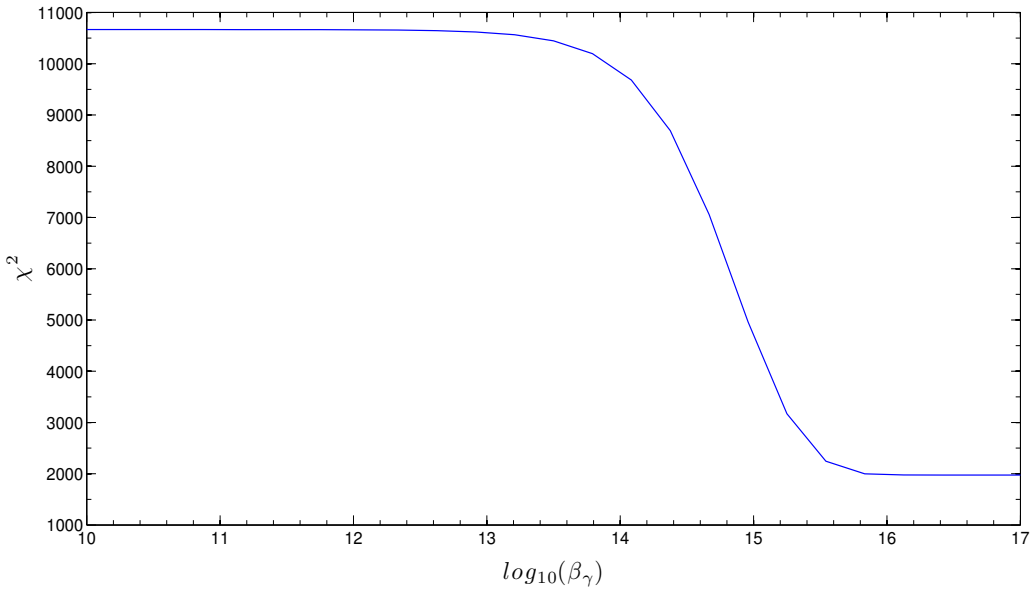

Figure 9: The χ^2 plot showing at what values of β_γ does the theoretical pulsar spectrum closely resembles the observed spectrum, where the lowest value of the χ^2 is obtained in the range $\beta_\gamma > 10^{16}$.

5.1.2 Oscillation probability

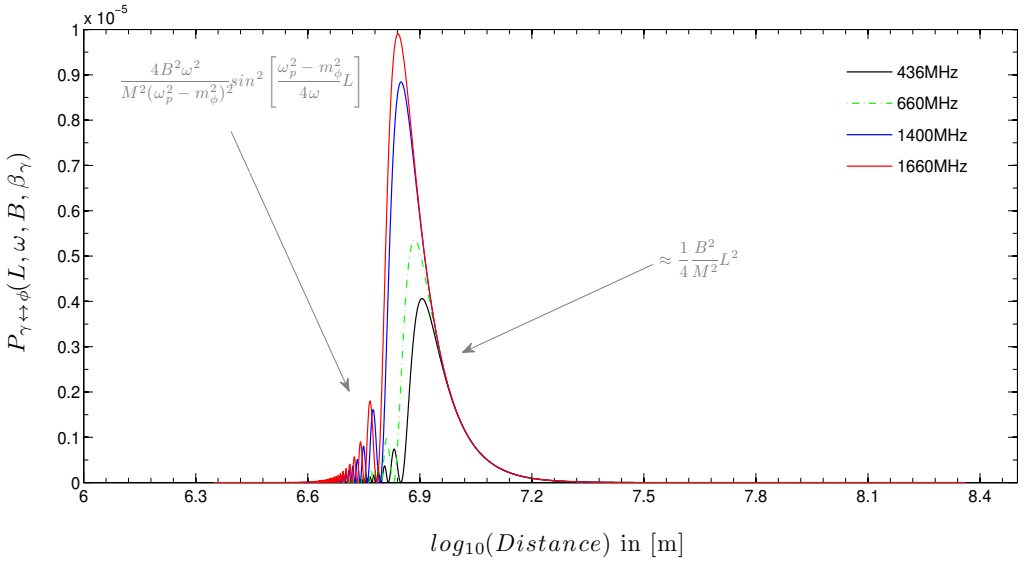

Figure 10: The plot of the chameleon-photon oscillation probability(vertical axis) versus the log of the propagation distance(horizontal axis) through a pulsar magnetosphere.

Figure(10) depicts the chameleon-photon oscillation probability at different photon frequencies and using $\beta_\gamma = 10^{17}$. For all the frequencies considered here one can see that there is one large prominent peak, before this peak we see an oscillatory behavior in which this peak is the last. The amplitude of this peak increases with the magnetic field strength B and the photon energy ω. These peaks occur at lower and lower altitudes as we increase in frequency, this is a consequence of the fact that high energy radio photons are emitted at lower altitudes compared to the low energy ones see equations (164 and 165).

This Near-Resonance-Peak (NRP) occurs where $|\omega_p - m_\phi| \approx 0$ see figure (10). Before

the NRP, the probability is given by the equation (128), from this equation it is clear that the probability amplitude is suppressed by the term $(\omega_p^2 - m_\phi^2)^2$ since both ω_p and m_ϕ increase with B, thus the spatial frequency $\frac{|\omega_p^2 - m_\phi^2|}{4\omega}$ is large, hence the chameleon-photon coherence length is short. After the NRP both ω_p and m_ϕ become very small compared to ω and their squares are even smaller, therefore the spatial frequency $\frac{|\omega_p^2 - m_\phi^2|}{4\omega}$ becomes small thus freezing the oscillations and the probability is given by equation (129). Since for pulsars, the far field magnetic field strength $B \propto \frac{1}{L^3}$, hence $P_{\gamma \leftrightarrow \phi} \propto \frac{1}{L^4}$ and is independent of photon energy ω, it drops rapidly with increase in L the propagation distance.

5.1.3 ω_p, m_ϕ and the mixing angle

From figure (11) one can see that the maximum mixing angle is $\pm 45°$ which is at NRP. At low altitudes ($< 10^7$m) the mixing angle is close to zero and increases to reach $45°$ at NRP, thus this is the weak mixing regime, while after the near resonance point the mixing angle for all the frequencies considered here is between $-40°$ and $-25°$, and this is the strong mixing regime.

Figure (12) depicts the chameleon mass and the plasma frequency as a function of propagation distance. We can see that before the NRP, the mass of ϕ is higher than ω_p and they become equal at the NRP. Once they have passed the NRP the chameleon mass falls below the plasma frequency, this is a result of the rapid decline of the magnetic energy density which the mass of ϕ depends on.

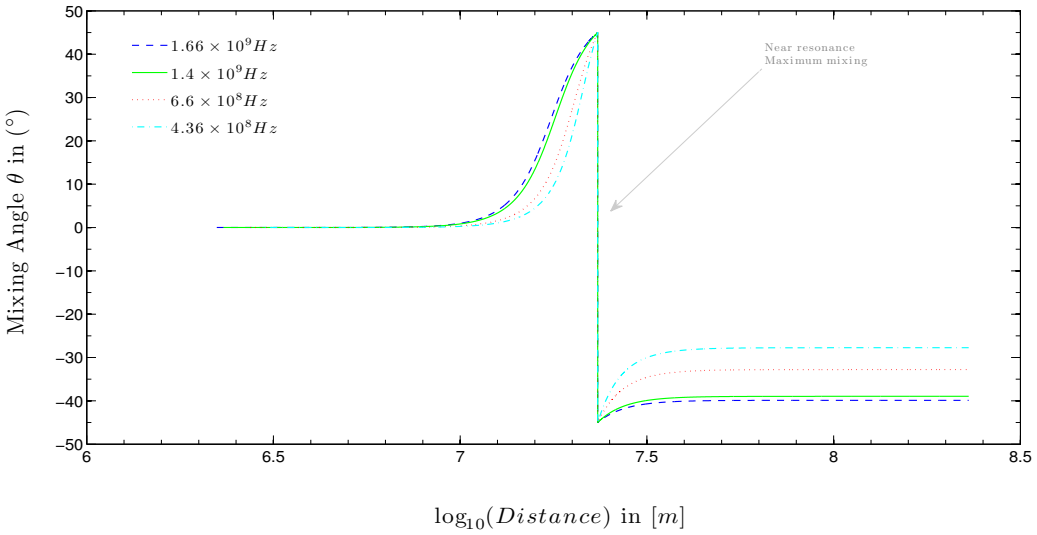

Figure 11: This plot shows the chameleon-photon mixing angle $\theta°$ versus the log of propagation distance for different photon energies.

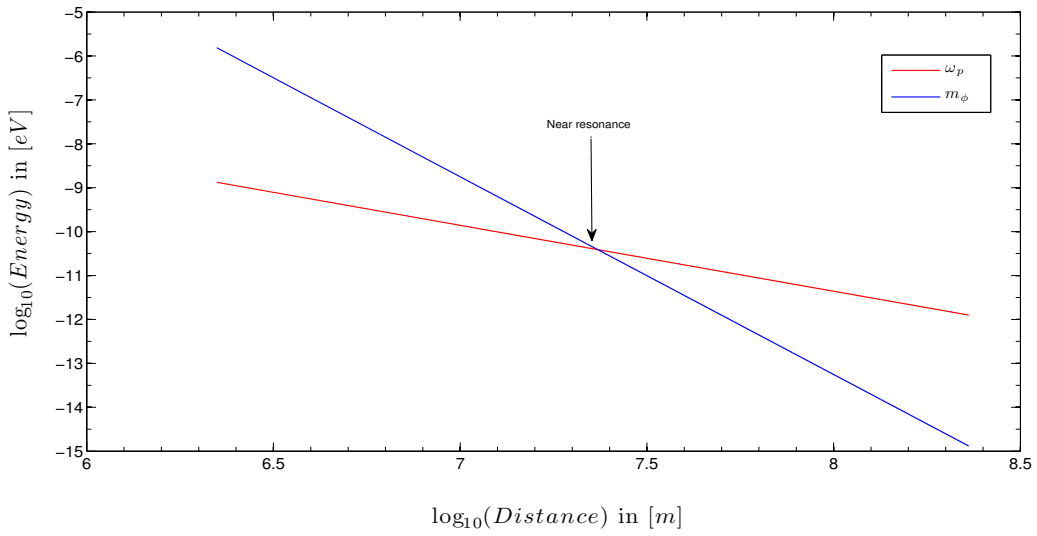

Figure 12: The plot of (m_ϕ) and (ω_p) as photons and chameleon particles propagate through a pulsar magnetosphere, the near resonance point is indicated.

5.1.4 Predicted and observed spectrum

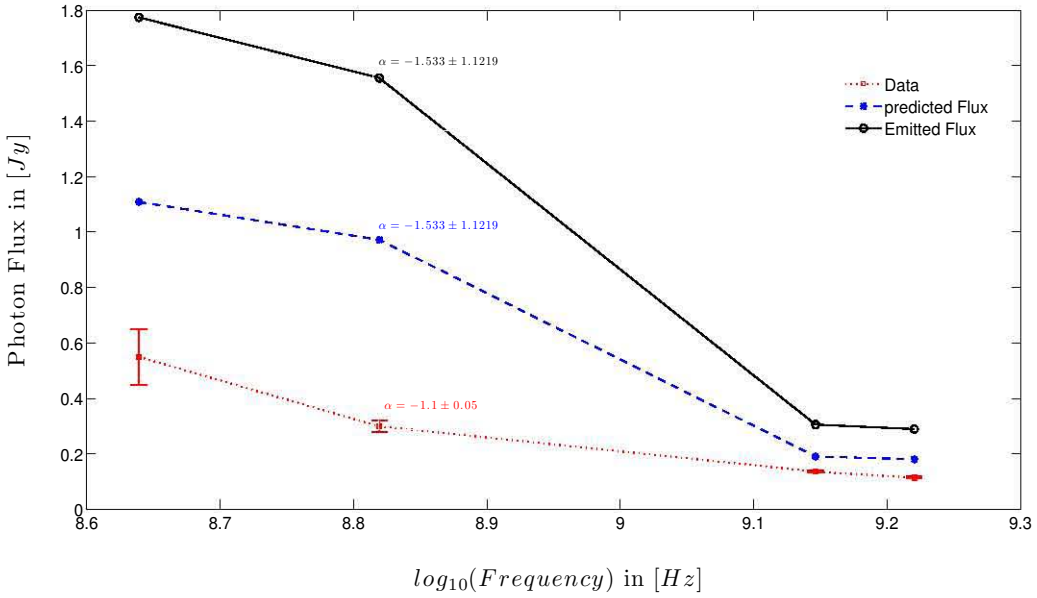

Figure 13: Here is a plot of photon flux versus log of frequency for the pulsar PSR J4037-4715, the red points with error bars indicate the observed data points, the blue points with stars show the predicted photon spectrum after chameleon-photon oscillations and the black points with circles show the initial theoretical emission spectrum, in this plot α indicates the spectral index.

In figure (13), we can see that the spectral index of the observed data (spectrum in red) is within the range of the predicted spectrum in blue and the shape of the spectrum is preserved from emission to detection after chameleon-photon mixing. The blue dashed spectrum was calculated using the coupling $\beta_\gamma = 10^{17}$, see figure (9). The black spectrum is the theoretical prediction of the emitted flux from the pulsar.

6 Discussion

6.1 Chameleon-photon oscillation probability

The chameleon-photon oscillation probability $P_{\gamma\leftrightarrow\phi}$ is given by equation (128), its amplitude is directly proportional to $\frac{4B^2\omega^2}{M^2(\omega_p^2-m_\phi^2)^2}$ in the weak mixing limit where we have that $\left|\frac{\omega_p^2-m_\phi^2}{\omega}\right| \gg \frac{B}{M}$. This means that $\frac{B\omega}{M|\omega_p^2-m_\phi^2|} \ll 1$, therefore the probability $P_{\gamma\leftrightarrow\phi} \ll 1$, hence the small values of the amplitude can be seen in figure (10) and it exhibits an oscillatory behaviour due to the large values of the spatial frequency $\frac{|\omega_p^2-m_\phi^2|}{4\omega}$ before the near-resonance-peak (NRP) is reached.

In order to improve on this we need large values of the coupling constant β_γ and photon energy ω while keeping the magnetic field strength B minimal, this is because large values of B lead to large values of $|\omega_p^2 - m_\phi^2|$ since $\omega_p^2 \propto B$ and $m_\phi^2 \propto B^3$, thus suppressing the probability amplitude. However, in the strong mixing regime where the oscillation probability is directly proportional to $(\beta_\gamma BL)^2$, clearly large values of B and propagation distance L at constant β_γ will increase the probability of chameleon-photon mixing.

6.2 β_γ constraints from pulsar flux

From figure (8) and subsequently figure (9), it is evident that significant reduction of flux in pulsar radio emission due to chameleon-photon mixing requires values of $\beta_\gamma > 10^{13}$, this is a result of the fact that pulsars have very large magnetic fields with small homogeneity scale length, thus for $\beta_\gamma < 10^{13}$ the chameleon-photon oscillations are suppressed.

At low altitudes in the pulsar magnetosphere the probability exhibits oscillations with low amplitudes, which is indicative of very short chameleon-photon coherence length.

This happens because the magnetic field changes rapidly, and has a very short homogeneity length scale. At high altitudes (above the NRP) the probability shows no oscillatory behaviour, this is because of long coherence length, which results in efficient mixing. But this homogeneous B field is small since $B \propto \frac{1}{L^3}$ where L is the distance from the pulsar. Therefore, the magnetic field drops rapidly with distance giving an overall decrease in the probability amplitude. Also, since we focused our calculations in the radio regime(low energy), the effects of mixing are suppressed.

6.3 Chameleon mass m_ϕ and the mixing angle θ

The mass of the chameleon (m_ϕ) and the plasma frequency (ω_p) which the probability ($P_{\gamma\leftrightarrow\phi}$) depends on so strongly are given by equation (35) and (163). Figure (12) shows how these two quantities change as the two particles (photon and chameleon) propagate through the pulsar magnetosphere. Before the near-resonance point indicated in figure (12) the mass of the chameleon is higher than the plasma frequency and this is due to the high energy density near the pulsar (chameleon effect), but photons couple and mix with light scalar particles and as a result, the probability is suppressed in this region [20].

However, after the near-resonance point, the mass of the chameleon becomes increasingly lower than the plasma frequency, in this region starting at a distance$> 10^{7.4}$m measured from the center of the neutron star, the mass (m_ϕ) is low enough, hence better

ϕ-photon oscillations occur, the amplitude of the probability is still small since the magnetic field has dropped significantly.

Figure (11) shows the mixing angle (θ) that can be calculated from equation (58), as we can see that close to the pulsar where distance$< 10^7$m the mixing angle (θ) is close to zero, and since the amplitude of the probability is proportional to $\sin 2\theta$, this confirms that the mixing is suppressed in this region. For distance$> 10^7$m the mixing angle increases to reach 45° at near-resonance, which gives the maximum value for $\sin 2\theta$. After this point there is a decline of no more than 20° at all the frequencies considered here, also confirming good mixing in this region.

6.4 Photon flux

Assuming that initially the chameleon flux is zero ($I_\phi(0) = 0$), then the incoming photon flux after chameleon-photon mixing will be reduced, the amount of reduction will depend on the oscillation probability and the number of magnetic domains that the photons actually pass through. In the case where there are initially equal amounts of photons and chameleons no change in the flux will occur, while if we start with a high chameleon than the photon flux, we will get an increase in the photon flux. In our case here, we have considered the case where $I_\phi(0) = 0$, thus the oscillations lead to a reduction of the photon flux, see figure (13).

In figure (13) the most important feature is the spectral index, because the magnitude of the flux can be biased depending on the model of pulsar radio emission one used, and

what telescope was used to do the observations. Therefore the slope of the log-log plot of the spectrum (i.e spectral index) is an invariant quantity with respect to the flux because at all frequencies the flux seen at the observer has been reduce buy the same amount.

7 Conclusions

7.1 Chameleon-photon oscillation probability in pulsars

The chameleon to photon oscillation probability in pulsars is not as large as one might naively expect, even though pulsars have very high magnetic fields. This high magnetic field causes problems because the plasma density and the effective mass of the chameleon both depend on it directly, hence near pulsars the chameleon mass is large, which suppresses the oscillation probability. The magnetic fields of pulsars far away from the surface can be approximated by that of a dipole, which is homogeneous over very short distances and this is bad for chameleon-photon oscillations. The only exception is at the near-resonance point which happens at a very short distance range.

7.2 Emission spectrum of pulsars

Figure (13) depicts the observed spectrum in red for the pulsar, the theoretically predicted emission spectrum in black without chameleon-photon oscillations and the predicted spectrum in blue including chameleon-photon oscillations. However, the blue line is closer to the observed data (red) than the black one. This discrepancy in the observed flux and the emitted flux could be explained by the following two reasons, it could be that either the theory of the emission mechanism in pulsars (in the radio) is not fully understood or just simply wrong, or photons get emitted and as they propagate through the pulsar magnetosphere and the interstellar medium (ISM) they get absorbed. Since after including chameleon-photon mixing, where photons can be converted to chameleons, we see a reduction in flux, this could be used to explain this discrepancy.

7.3 Constraints on β_γ

We require very high values of the coupling in the range $\beta_\gamma > 10^{13}$ (see figure 8 and 9), in order to have any observable effect on the pulsar spectrum. In this discussion we restricted ourselves to values of the chameleon-matter coupling β_m of $\mathcal{O}(1)$, which does not overlap with any existing laboratory experiment. There is still a wide range of β_ms to explore.

7.4 Recommendations and future work

For a full treatment of chameleon interactions, we need to include the chameleon-matter coupling β_m constraints since the chameleon couples to fermions as well. We need to also use different models for the chameleon potential (the functional form of the potential) to to fully constrain the theory. One can also include vacuum polarization effects due to electron positron pair production in the magnetospheres of pulsars which were assumed to be small in this discussion.

High quality observations using MeerKAT, ALMA and the SKA telescopes are needed to improve the quality of the spectral data of pulsars in the radio regime, such that better simulations of pulsar spectra can be done. In the near future this work could me extended to quasars and galaxy clusters where magnetic fields are present and have very long homogeneity scale lengths.

References

[1] Khoury J, Weltman A. "Chameleon cosmology". *Phys Rev D.* 2004 Feb;69(044026)(arXiv:astro-ph/0309300v3).

[2] Khoury J, Weltman A. "Chameleon Fields: Awaiting Surprises for Tests of Gravity in Space". *Phys Rev Lett.* 2004 Oct;93(171104)(arXiv:astro-ph/0309300v3).

[3] Brax P, van de Bruck C, Davis AC, Khoury J, Weltman A. "Chameleon Dark Energy". *AIP ConfProc.* 2004 Oct;736(arXiv:astro-ph/0410103v1):pp. 105–110.

[4] Weltman A. "Testing Chameleon Models in the Laboratory". *43rd Rencontres de Moriond: Cosmology.* 2008 Mar;(arXiv:0805.3461v1 [hep-ph]).

[5] Steffen JH. "The CHASE laboratory search for chameleon dark energy". *PoS* . 2010 Nov;ICHEP2010(arXiv:1011.3802v2 [hep-ex]):pp. 446–452.

[6] Einstein A. "Cosmological Considerations in the General Theory of Relativity". *SitzungsberPreussAkadWissBerlin (MathPhys).* 1917 Feb;1917(-):pp. 142–152.

[7] Eddington A. "On the instability of Einsteins spherical world". *Mon Not Roy Ast Soc.* 1930 May;90(11):pp. 668–678.

[8] Zeldovich Y. "Cosmological constant and elementary particles". *Sov Phys JETP Lett.* 1967;6:pp. 316–317.

[9] Zeldovich Y. "The cosmological constant and the theory of elementary particles". *SovPhysUsp.* 1968 Mar;11(7):pp. 381–393.

[10] Guth A. "Inflationary universe: A possible solution to the horizon and flatness problems". *Phys Rev D*. 1981 Jan;23(2):pp. 347–356.

[11] Schmidt BP, et al. "The High-z Supernova Search: Measuring Cosmic Deceleration and Global Curvature of the Universe Using Type Ia Supernovae". *The Astrophysical Journal*. 1998 Nov;507(1)(arXiv:astro-ph/9805200v1):pp. 507–546.

[12] Perlmutter S, et al. "Measurements of Ω AND Λ From 42 High-Redshft Supernovae". *The Astrophysical Journal*. 1999 Jun;517(2)(arXiv:astro-ph/9812133v1):pp. 565–586.

[13] Ellis GFR. "A historical review of how the cosmological constant has fared in general relativity and cosmology". *Chaos, Solitons and Fractals*. 2003 May;16(4):pp. 505–512.

[14] Riess A, et al. "Observational Evidence from Supernovae for an Accelerating Universe and a Cosmological Constant". *Astronomical Journal*. 1998 Sept;116(3)(arXiv:astro-ph/9805201v1):pp. 1009–1038.

[15] Spergel D, et al. "First-Year Wilkinson Microwave Anisotropy Probe (WMAP) Observations: Determination of Cosmological Parameters". *The Astrophysical Journal Supplement Series*. 2003 Sept;148(1)(arXiv:astro-ph/0302209v3):pp. 175–194.

[16] Ratra B, Peebles PJE. "Cosmological consequences of a rolling homogeneous scalar field". *Phy Rev D*. 1988 Jun;37(12):pp. 3406–3427.

[17] Webb JK, et al. "Does the Fine Structure Constant Vary? a Third Quasar Absorption Sample Consistent With Varying α". *Astro & Space Science*. 2003 Mar;283(4)(arXiv:astro-ph/0210531v1):pp. 565–575.

[18] Bekenstein JD. "Fine-structure constant: Is it really a constant?". *Phys Rev D.* 1982 Mar;25(6):pp. 1527–1539.

[19] Dvali G, Zaldarriaga M. "Changing α withTime: Implications for Fifth-Force-Type Experiments and Quintessence". *Phys Rev Lett.* 2002 Mar;88(091303)(arXiv:hep-ph/0108217v1).

[20] Raffelt G, Stodolsky L. "Mixing of photons with low mass particles". *Phys Rev D.* 1988 Mar;37(5):pp. 1237–1249.

[21] Burrage C, Davis A, Shaw DJ. "Detecting Chameleons: The Astronomical Polarization Produced by Chameleon-like Scalar Fields". *Phy Rev D.* 2009 Feb;79(044028)(arXiv:0809.1763 [astro-ph]).

[22] Burrage C. "Supernova Brightening from Chameleon-Photon Mixing". *Phys Rev D.* 2008 Feb;77(043009)(arXiv:0711.2966v1 [astro-ph]).

[23] Gies H, Mota DF, Shaw DJ. "Hidden in the light: Magnetically induced afterglow from trapped chameleon fields". *PhysRev D.* 2008 Jan;77(025016)(arXiv:0710.1556 [hep-ph]).

[24] Ahlers M, Lindner A, Ringwald A, Schrempp L, Weniger C. "Alpenglow-a signature for chameleons in axion like particle search experiments". *PhysRev D.* 2007 Oct;77(015018)(arXiv:0710.1555 [hep-ph]).

[25] Upadhye A, Steffen JH, Weltman A. "Constraining chameleon field theories using the GammeV afterglow experiments". *PhysRev D.* 2010 Mar;81(015013)(arXiv:0911.3906v1 [hep-ph]).

[26] Waterhouse TP. "An Introduction to Chameleon Gravity". 2006 Nov;(arXiv:astro-ph/0611816v1).

[27] Chelouche D, et al. "Spectral Signatures of Photon-Particle oscillations from celestial objects". *The Astrophysical Journal Supplement Series*. 2009 Jan;180(arXiv:0806.0411v1 [astro-ph]):pp. 1–29.

[28] Gaensler BM, Bock DCJ, Strappers BW. "Non-Detection of a Pulsar-Powered Nebula in Puppis A, and Implications for the Nature of the Radio-Quiet Neutron star RX J0822-4300". *The Astrophysical Journal*. 2000 Jul;537(arXiv:astro-ph/0003032v2).

[29] Toscano M, Bailes M, Manchester RN, Sandhu JS. "Spectra of Southern Pulsars". *The Astrophyical Journal*. 1998 Oct;506(2)(arXiv:astro-ph/9805241v1):pp. 863–867.

[30] Wilson TL, Rohlfs K, H*ü*ttemeister S. "Tools of Radio Astronomy". 5th ed. *Springer*; 2009.

[31] Venter C, Jager OCD. "Spectral Constraints for Millisecond Pulsars due to General Relativistic Frame Dragging". *Astrophysics and Space Science*. 2005 Jun;297(1-4):pp. 399–407.

[32] Kijak J. "Emission Altitude in Radio Pulsars". *270th WE-Heraeus Seminar on Neutron Stars, Pulsars and Supernova Remnants*. 2002 Aug;(MPE-REPORT-278)(arXiv:astro-ph/0208561v1).

[33] Kijak J. "Emission altitudes in young and old radio pulsars". *MonNotRoyAstronSoc*. 2001 Jan;323(arXiv:astro-ph/0101429v2):pp. 537–541.

[34] Gil J, Krawczyk A, Melikidze G. "Pulsar Radiation". *Mathematics of Gravitation Part II, Gravitational wave Detection Banach Center Publications.* 1997;41(2):pp. 239–255.

[35] Melikidze GI, Gil JA, Pataraya AD. "The spark-associated soliton model for pulsar radio emission". 2000 Feb;(arXiv:astro-ph/0002458v1).